Journal of Materials Chemistry C

ROYAL SOCIETY OF CHEMISTRY

REVIEW

View Article Online
View Journal | View Issue

Cite this: J. Mater. Chem. C, 2025, 13, 19927

2D and layered materials for bio-integrated devices: insights into their multiscale interaction with biological moieties

Nabila Yasmeen,[a] Nada Morsy,[a] Mariam Badawi,[b] Roberta Gagliani,[d] Sung Mun Lee,[a] Emmanuel Stratakis,[c] Lucia Gemma Delogu,[de] Yarjan Samad[f] and Anna-Maria Pappa *[acgh]

Received 14th March 2025,
Accepted 3rd September 2025

DOI: 10.1039/d5tc01114k

rsc.li/materials-c

Two-dimensional (2D) and layered materials have successfully advanced the energy and electronics sectors, providing high translational capacity. However, when it comes to biomedical applications, their full potential is yet to be fully explored. This limitation can be attributed to the lack of fundamental understanding of the interactions that govern the behavior of these materials in the biological environment. Such understanding would not only open access to novel forms of biological-2D material hybrids but could also provide insights into nano-scale machinery by which biological domains function. This review highlights the current progress in developing 2D and layered material-based biointerfaces and their respective interactions with biological systems across different length and complexity levels. We first review the various interface modification, functionalization, and processing methods employed to enhance such biointerfacing for high-performing biomimetic devices (including electronic and optical devices). We then discuss the different types of interactions across the interface and finally the biotransducer-junction mechanisms taking place, at the device-performance level.

1. Introduction

Two-dimensional (2D) and layered materials are crystalline materials of one- or two-atom-thick layered configuration with relatively weak van der Waals interactions that potentially separate the material into distinct, freestanding layers.[1,2] Their unique configuration allows for engineering properties at the atomic scale thereby enabling a versatile design space for a variety of applications notably in the energy and electronics sectors.[3] The global market for 2D and layered materials is growing at a compound annual growth rate (CAGR) of 3.9%, which is expected to reach nearly USD 3.19 billion by 2030[4] across various commercial applications. Notably, the global market for graphene is anticipated to reach USD 1.64 billion by 2034, representing a 27% CAGR over the next decade.[4] Many graphene-based inventions have seen commercial success so far, with the award-winning 2-DTECH Graphene Company (North America) being a characteristic example for the production of graphene at scale and for graphene-based device prototyping.[5]

Indeed, graphene's unique combination of properties, such as tensile strength, electronic mobility, thermal conductivity, and surface chemistry, makes it a highly versatile material for a wide range of applications. These include biomedical devices such as biosensors, bio-robotics, and wearable technologies.[6–10] Despite the ever-increasing number of publications in the biomedical field, the pathway to commercialization is yet to be fully explored in part due to the stringent regulations but also due to a lack of proper understanding of the intricate bio-interface between biological systems and 2D materials.

Beyond graphene, other two-dimensional (2D) materials, including graphene oxide (GO), hexagonal boron nitride (h-BN), transition metal dichalcogenides (TMDs), black phosphorus (BP), layered metal oxides (LMOs), and MXenes, have garnered significant attention due to their exceptional properties and potential applications.[11–19]

Graphene oxide (GO) is a chemically modified derivative of graphene, featuring tunable surface chemistry that enables its use in various bio-interface applications.[20–22] Hexagonal boron

[a] Department of Biomedical Engineering and Biotechnology Khalifa University of Science and Technology, Abu Dhabi, United Arab Emirates. E-mail: anna.pappa@ku.ac.ae
[b] Department of Mechanical Engineering, Khalifa University, United Arab Emirates
[c] Institute of Electronic Structure and Laser (IESL), Foundation for Research and Technology-Hellas Crete, Greece
[d] Department of Biological Sciences, Khalifa University of Science and Technology, Abu Dhabi, United Arab Emirates
[e] Department of Biomedical Science, University of Padua, Padua, Italy
[f] Department of Aerospace Engineering, Khalifa University, United Arab Emirates
[g] Center for Catalysis and Separations, Khalifa University, United Arab Emirates
[h] Center for Biotechnology, Khalifa University of Science and Technology, Abu Dhabi, United Arab Emirates

nitride (h-BN) is a dielectric material with structural and physical similarities to graphene, exhibiting high mechanical strength, excellent electronic mobility, and superior chemical and thermal stability with applications in lubricants and protective coatings[18] and more recently in biomedical applications.[23] Transition metal dichalcogenides (TMDs), including molybdenum disulfide (MoS_2) and tungsten disulfide (WS_2), present tunable bandgaps and semiconducting properties, making them ideal for applications in electronic devices including transistors and photodetectors.[19,24] Black phosphorus (BP), characterized by a tunable bandgap as well, exhibits high carrier mobility, anisotropic in-plane properties and intrinsic biodegradability, with its use in diverse device formats including field-effect transistors (FETs), optoelectronic devices,[25] and photoacoustic imaging tools.[26] Layered metal oxides (LMOs) feature unique electrochemical properties, thermal stability, mechanical strength, and catalytic activity.[27] Their high cycling stability makes them highly effective as cathode materials in lithium-ion batteries,[28,29] whereas magnetic layered oxides, such as iron oxides, serve as contrast agents in magnetic resonance imaging (MRI). Last but not least, MXenes (Mn + 1XnTx) represent a broad class of 2D materials characterized by a structure comprising two or more layers of transition metal (M) atoms arranged in a honeycomb-like lattice, intervened with layers of carbon and/or nitrogen.[30] Among the various types, titanium carbide and tantalum carbide have shown excellent hydrophilicity, biodegradability, and low cytotoxicity rendering them suitable for diverse biomedical applications[31] and advanced medical diagnostics, military technologies, and optical communication systems.[32]

Overall, 2D and layered materials exhibit a broad applicability spectrum across various fields as shown in Fig. 1.[33,34] An earlier perspective, ''Graphene Devices for Life'',[35] outlines the promise of the bio-nano interface of 2D materials, particularly graphene and graphene oxide, in biomedical applications, emphasizing how surface chemistry governs their interactions with biological systems.[36,37] It highlights the need for comprehensive studies on biocompatibility, bio-interface dynamics, and the translational pathways required for successful clinical implementation. While recent reviews provide critical insights into the biological fate of 2D materials in *in vivo* scenarios, there remains a gap in the mechanistic understanding of the bio-transducer junctions formed, encompassing their biological identity, interaction mechanisms, and bio-interface engineering strategies. This review systematically examines recent advancements in understanding these interactions at varying length and complexity levels in biology. It also aims to establish design criteria for 2D and layered materials, facilitating their integration into highly performing bio-integrated devices.

2. 2D and layered materials: synthesis, processing, and device integration

Using different synthesis and functionalization approaches, 2D and layered materials can be tuned *via* tailoring their size, number of layers, surface-to-volume ratio, defects, *etc.*[38] This enables optical and electrical performance diversity, impacting the resulting devices and the potential application areas. The fabrication of 2D materials can be classified into top-down and bottom-up approaches as shown in Fig. 2. Top-down methods involve breaking down the bulk layered materials into thinner nanosheets. In contrast, bottom-up methods involve synthesizing 2D materials from atomic or molecular precursors.[39]

2.1 Bottom-up approach

Bottom-up synthesis strategies construct two-dimensional (2D) materials directly from atomic or molecular precursors, enabling precise control over structural and functional properties. Techniques such as chemical vapor deposition (CVD), atomic layer deposition (ALD), epitaxial growth, thermal pyrolysis, laser-assisted synthesis, and wet-chemical routes have been widely explored.[40–42] These methods allow for tailored engineering of 2D architectures with tunable thickness, crystallinity, and chemical composition. Among them, CVD offers precise thickness control and the ability to produce large-area, high-quality films, including vertical and lateral heterostructures, suitable for applications in electronics, optoelectronics, sensing, flexible devices, and catalysis.[43–47] Although bottom-up methods are often constrained by complex equipment requirements and limited throughput, innovations such as roll-to-roll CVD systems are addressing scalability challenges.[48] Recent advances extend beyond conventional CVD, including methane cracking *via* thermal catalysis, molten media, or plasma cracking,[49] as well as the controlled explosion of aromatic hydrocarbons such as benzene and toluene.[50] Emerging approaches, such as laser-assisted CVD, further expand the capabilities of bottom-up synthesis. By locally heating substrates or precursor gases with a focused laser beam, this method enables precise microscale patterning and the direct integration of 2D materials onto flexible electronic substrates.[51,52] Overall, adjustments in bottom-up synthesis techniques can achieve scalable, high-quality 2D materials with properties tailored for advanced technologies and device integration.

2.2 Top-down approach

Top-down synthesis relies on the systematic fragmentation of bulk layered materials into nanoscale sheets, offering a practical route for large-scale production. Compared to bottom-up methods, these approaches are generally more scalable and cost-effective, making them attractive for commercial applications. A diverse range of techniques have been developed, including mechanical methods such as ball milling[53] chemical oxidation—reduction exfoliation,[54] liquid phase exfoliation (sonication,[55] high-shear mixing,[56] microfluidization,[57] high-pressure homogenization,[58] wet ball milling,[59] and Taylor–Couette flow[60]), as well as electrochemical exfoliation.[61] By enabling the production of nanosheets and nanoparticles in macroscale quantities, top-down approaches overcome the limited throughput of bottom-up synthesis. The resulting 2D materials have found use in conductive inks, with liquid-phase exfoliated graphene inks already demonstrated in touch-screen sensors, wireless antennas, and flexible electronics.[62,63] Wet-jet milling, a scalable liquid-phase exfoliation technique,[64] has been successfully commercialized for producing graphene-

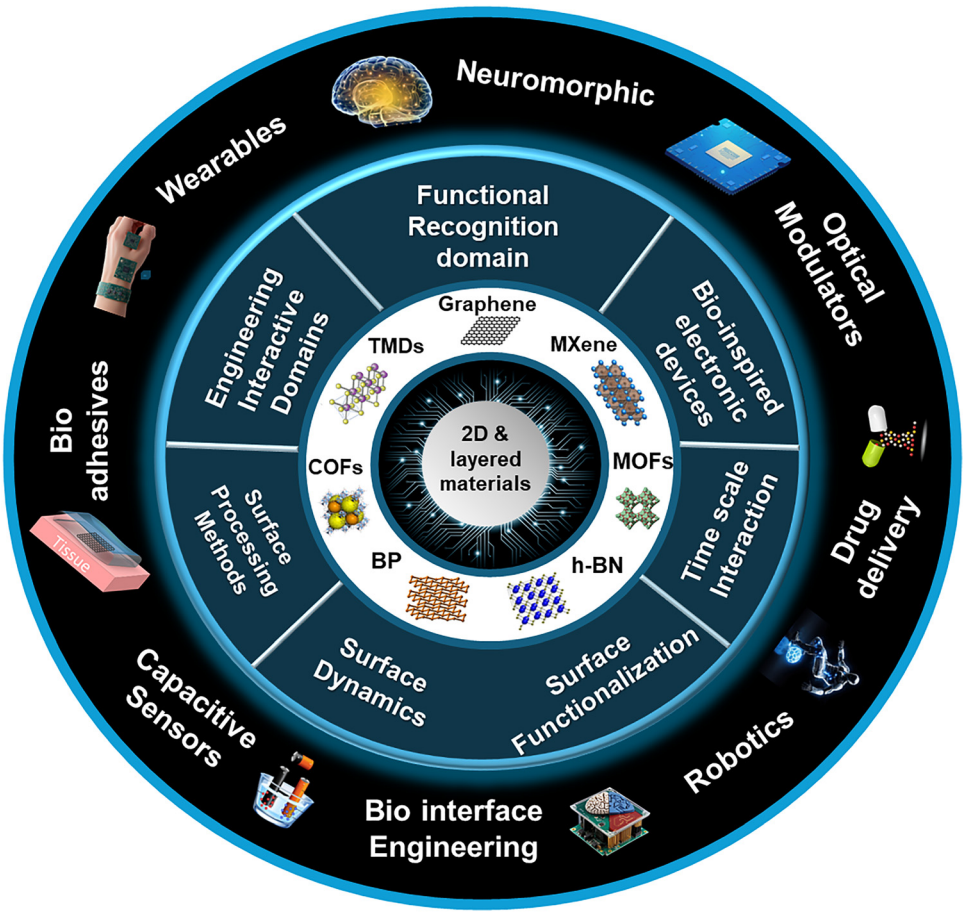

Fig. 1 A simplistic schematic representation of the applications of 2D and layered materials in biomedicine (created in https://www.freepik.com).

based inks used in anti-corrosion coatings, highlighting the industrial potential of top-down fabrication strategies.[65,66]

2.3 Eco-friendly processing approaches

Eco-friendly processing strategies for two-dimensional (2D) materials are gaining attention as they minimize bio-interfacial toxicity and improve colloidal stability, enabling accurate and systematic biological data assessment.

Green solvents derived from gallnut and coffee waste extracts have been employed for 2D layer functionalization, assisting cavitation-driven exfoliation of bulk precursors into nanosheets.[67] To obtain few-layer or monolayer boron nitride nanosheets from bulk hexagonal boron nitride without relying on harsh organic solvents such as NMP or DMF, or toxic reducing agents, a glucose-assisted ultrasonic cavitation strategy has been demonstrated.[68] Functionalization of graphene with polyphenolic compounds from beetle extracts has yielded layers exhibiting antibacterial and anticancer activity, alongside high crystallinity and low defect density. Similarly, bovine serum albumin has been used to functionalize graphene surfaces, effectively suppressing nonspecific binding and enabling selective electrochemical sensing.[69] Bio-inspired methods such as liquid-phase exfoliation with biomolecular exfoliants such as peptides are also emerging.[70] The exfoliated sheets can be stabilized by acid–base interactions between the nucleotide's phosphate groups and the nanosheet surfaces, retaining their catalytic properties for hydrogen evolution reactions, demonstrating that biofunctionalization does not compromise their functional performance (Fig. 3(a)).[71] In another example, processing graphene in a kitchen blender using animal sera (bovine, chicken, human, horse, porcine, and rabbit) resulted in highly stable graphene flakes (0.5–1 μm, $\sim$2.0 mg mL^{-1} h^{-1}) without requiring post-processing. In this case, protein corona formation enhances dispersibility, stability, and biocompatibility relative to conventional surfactant-based methods, likely by passivating the hydrophobic graphene surface (Fig. 3(b)).[72] Onion-like graphene/MoS_2 nanosheets can be fabricated using a one-pot plasma-induced method involving two simple electrolysis plasma steps. This chemical-free, energy-efficient approach avoids the use of harsh solvents or reagents, underscoring its eco-friendly nature. The resulting nanosheets demonstrated high electrical conductivity and stable electrocatalytic performance without detectable degradation, highlighting the potential of plasma-based green processing for scalable 2D material synthesis (Fig. 3(c)).[73] An additional eco-conscious strategy is the efficient one-step mechanical exfoliation method for MXene synthesis. This process combines ball milling with mild acidic etching under a nitrogen-

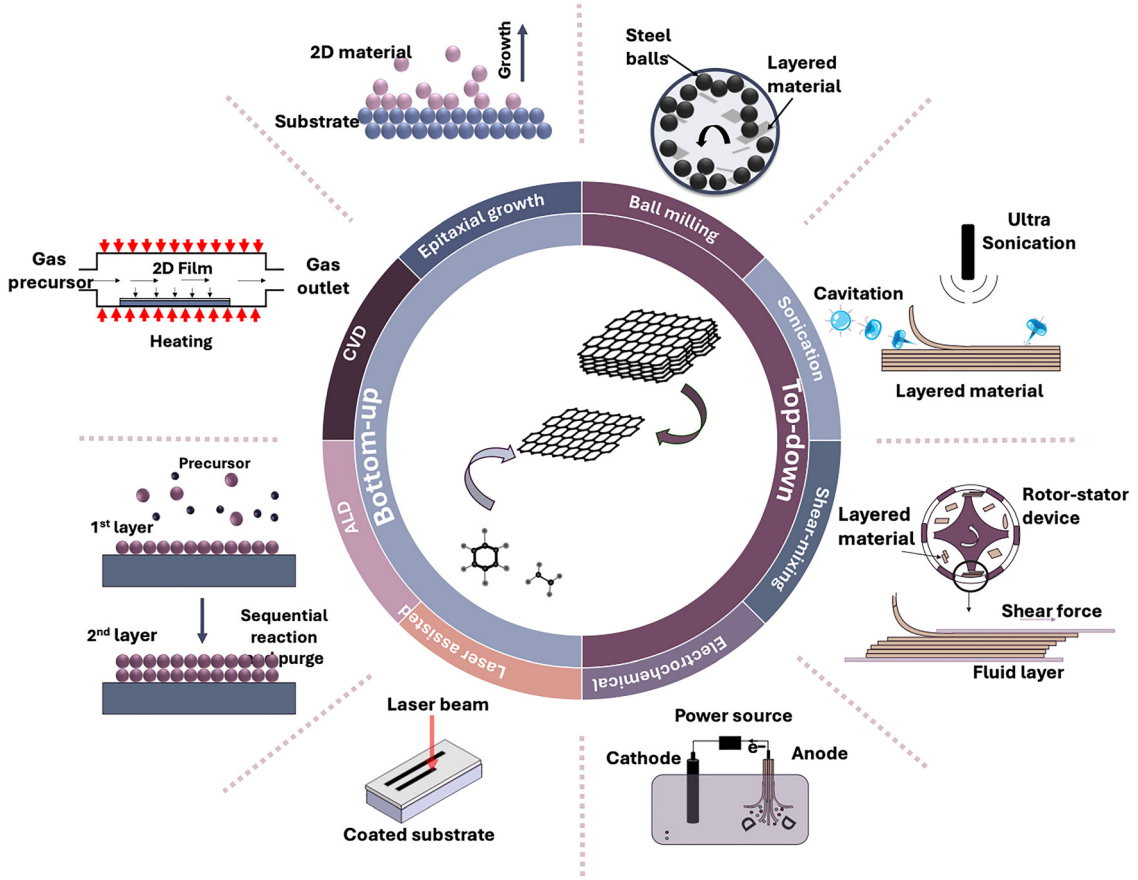

Fig. 2 2D and layered material synthesis: bottom-up and top-down approaches.

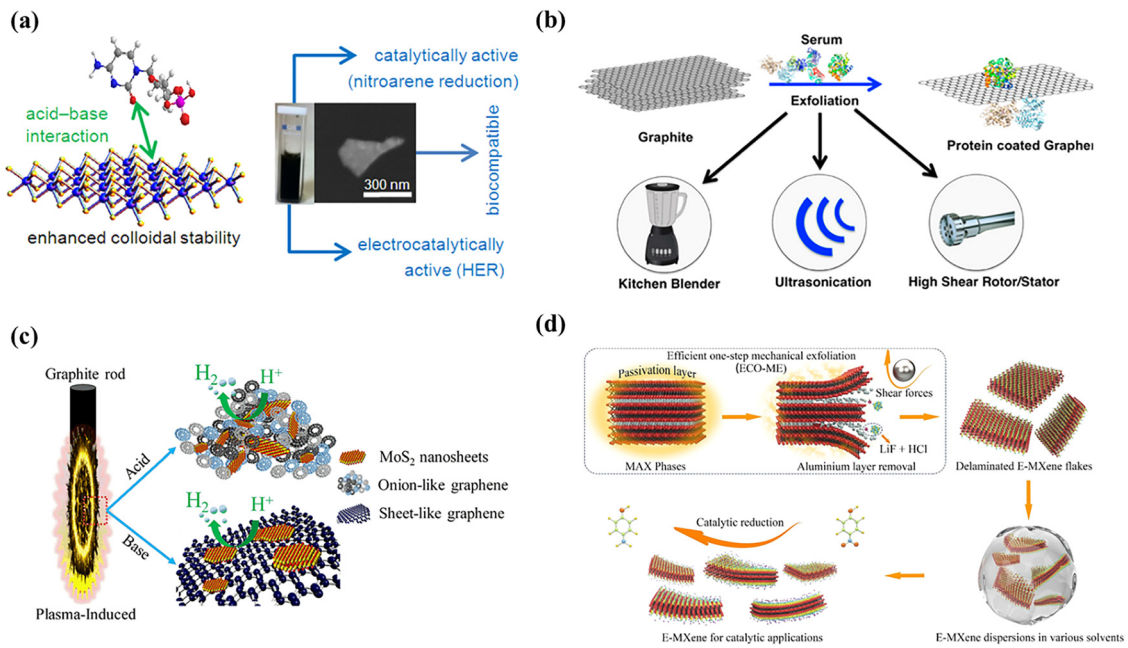

Fig. 3 Schematic illustration of green processing methods for 2D material fabrication. (a) DNA–RNA assisted MoS_2 exfoliation (copyright 2017 *ACS Appl. Mater. Interfaces.*).[71] (b) Kitchen blender method for graphene synthesis in *Caenorhabditis elegans* (copyright 2017 *Langmuir*).[72] (c) Schematic representation of the proposed mechanism of OGNs@MoS_2 and GNs@MoS_2[73] (copyright 2020 ACS Appl. Mater. Interfaces.). (d) ECO-ME synthetic pathway for the preparation of MXenes (copyright 2023 *Chem. Eng. J.*).[74]

purged atmosphere, enabling the rapid, scalable production of MXene nanosheets with large lateral dimensions, offering a sustainable route to high-quality nanosheets (Fig. 3(d)).[74]

2.4 Bio-integrated devices

In the field of bio-integrated devices, 2D materials have driven progress in both optical and electrochemical platforms, with key examples summarized in Table 1. Among biomedical applications, field-effect transistor (FET) sensors, electrochemical sensors, fluorescent sensors, and bioadhesives are the most extensively explored. For biosensing applications, the intrinsic properties of 2D materials, *i.e.*, their large surface area and tunable surface chemistry, facilitate efficient immobilization of bioreceptors, imparting molecular specificity while maintaining high sensitivity. This has enabled rapid and reliable detection of diverse biomolecules, from nucleic acids to proteins, with performance metrics surpassing many conventional sensing platforms. Beyond sensing, 2D materials have also been investigated as advanced bioadhesives. Their mechanical flexibility, stretchability, and intrinsic durability, combined with biocompatibility, enhance their conformal contact with biological tissues for applications in wound dressings, wearable devices, and implantable systems. In such cases, both adhesiveness and biocompatibility are essential, which can be tailored using material engineering routes.

3. 2D and layered material interactions across varying length and complexity levels

The interactions of 2D and layered materials with biological systems are shaped by multiple factors including biological identity, interaction timescale, spatial interaction range, surface chemistry, and environmental conditions, all of which collectively determine the interface dynamics, binding specificity, and functionality. Compared with both lower- and higher-dimensional nanostructures, 2D materials possess exceptionally high surface-to-volume ratios, making surface forces particularly critical for their integration into bioelectronics and biomedical devices. Their planar morphology offers an extended surface area, which enhances molecular adsorption relative to curved nanostructures. As curvature decreases, adsorption capacity increases, with van der Waals interactions becoming more energetically favorable, thereby strengthening biomolecular binding.[91,92,93]

3.1 Material–biological interfacing across various dimensional architectures

The interaction of nanomaterials with biological systems is strongly influenced by their dimensional architecture, which dictates surface chemistry, electronic behavior, and mechanical adaptability. Understanding how materials across 0D, 1D, and

Table 1 Summary of bio-devices utilizing different 2D materials and their functions and additional features

Bio-device	2D material	Sensing/therapeutic functionality	Performance features	Ref.
Field-effect transistor sensors				
	Graphene sheets	SARS-CoV-2 spike protein	Limit of detection [LOD]: 1.6×10^1 pfu mL^{-1} (culture medium) 2.42×10^2 copies mL^{-1} (clinical sample)	75
	n-$MoTe_2$ and p-GeSe sheets	Streptavidin biomolecules	LOD: 5 pM	76
	MXene-CD9 aptasensor	Exosomes: CD9 proteins	LOD: 10.64 pM (buffer) 6.41×10^2 exosomes mL^{-1} (human serum)	77
	BP	Antibiotic sensing (tetracycline)	LOD: 7.94 nM	78
Electrochemical sensors				
	Pt/$Ti_3C_2T_x$ assembled with graphene	Dopamine	LOD: 50 nM	79
	Graphene quantum dots	Human immunodeficiency virus	LOD: 51.7 pg mL^{-1}	80
	MXene and MWCNTs	Amyloid β-protein	LOD: 0.3 fg mL^{-1}	81
	Covalent organic framework (COF)	Glutathione	LOD: 0.0093 nM	82
	Cu–metal–organic frameworks (MOF)	Biomolecules	LOD: ascorbic acid 2.94 μM LOD: H_2O_2 4.1 μM LOD: L-histidine 5.3 μM	83
Bio-adhesives				
	BP nanosheets	Wet-tissue adhesion	Rapid haemostasis (within ∼1–2 seconds)	84
	Self-powered chitosan/graphene oxide hydrogel band	Adhesive wound patch	Controlled electronic drug release as transdermal therapy	85
	Graphene integrated hydrogel	Multifunctional-stretchable bioelectronics	Fivefold stretchability boost; *in vivo* cardiac signal detection (caused by arrhythmia)	86
Fluorescent bio-devices				
	Fluorinated graphene oxide	*In vitro* cytotoxicity study	High-resolution biocompatible metal-free MRI nanoprobes	87
	MoS_2–EMAmer (ensemble-modified aptamer) sensor	Cancer diagnostics platform (complex media)	Discrimination among six types of cancer cells (10^4 cells within 60 min)	88
	Zwitterion-modified MXene	Sanguinarine drug encapsulation	Antibacterial effect against *Staphylococcus aureus* and *Escherichia coli*, wound healing efficiency	89
	BP	Photothermal and sonodynamic therapeutics	Antibacterial activity against *S. aureus* (96.6% *in vitro* and 97.3% *in vivo*)	90

2D scales engage with biological interfaces is critical for designing next-generation bioelectronic and biomedical devices. Zero-dimensional (0D) nanomaterials, such as quantum dots, interact with biological systems through their ultrasmall size and high surface reactivity, enabling precise molecular recognition and a highly tunable surface chemistry.[94] In contrast, one-dimensional (1D) nanomaterials such as nanowires or nanotubes exhibit quantum-confined electrical behavior, making their electronic responses highly sensitive to changes in biomolecular binding density and surface functionalization.[95] Their high surface-to-volume ratio also supports effective functional biointerfaces; for instance, indium phosphide nanowires have demonstrated the ability to transduce macromolecular interactions, such as bacterial adhesion, into detectable electronic or optical signals.[96] Two-dimensional (2D) layered materials offer broad surface contact, high carrier mobility, and facile functionalization, enabling precise signal transduction[97] and seamless integration with biological tissues.[97] These attributes not only enhance biorecognition sensitivity but also minimize inflammatory responses compared with rigid electrode counterparts.[98–100] In three-dimensional (3D) structures, interactions are governed by parameters such as surface charge, surface chemistry, particle size, specific surface area (SSA), and curvature. Importantly, 2D materials exhibit significantly larger SSAs, which scale with mass rather than size, a key distinction from 3D systems that makes them particularly well-suited for probing bio-nano interactions. However, their high surface area also amplifies intermolecular forces at the biological interface, which can drive biomolecular unfolding, compromise physicochemical and functional integrity, and ultimately alter the structural properties of the nanosheet. Beyond their intrinsic advantages, 2D materials can undergo dimensional transformations into 0D, 1D or 3D nanostructures, thereby combining the functional benefits of multiple architectures.

A summary of critical parameters governing biointerfacing across dimensional scales is provided in Table 2.

3.2 Biological identity

Biomolecules, such as proteins, nucleic acids, and lipids, possess intrinsic properties, including charge, hydrophobicity, and functional group distribution. Similarly, 2D materials have their own intrinsic properties, including crystallinity, defects, elasticity, conductivity, and thickness. These characteristics shape their ''biological identity'', *i.e.*, how 2D materials and biological moieties interact; the interaction is a dynamic exchange where both components contribute to the conjugated system's behavior and function.

One way to visualize the extent of the interaction between 2D materials and biological systems is by examining their similarities, such as affinity arising from mechanical compatibility and structural factors (bond lengths and positions), matching polarities (hydrophilicity), complementary surface charges, functional groups, and compatible Hansen solubility parameters (HSPs); HSPs serve as an indicator for monitoring the biomolecule and 2D material surface interactions.[118] Such interactions create a unique biological fingerprint for each 2D material and influence biomolecules' diffusion and adsorption rates on the material's surface.

The Hansen parameters assess the energy needed to disperse one component into another119 and are related to the dispersive, polar, and hydrogen bonding contributions to the cohesive energy density of the material.[120] The dispersive (δD), polar (δP), and H-bonding (δH) interactions of some 2D materials and biomolecules are presented in Table 3. Using these values, parameter R_a (Table 3), which is a measure of the HSP distance between two molecules, conventionally how alike they are, can be determined using values from Table 1 and the equation $R_a^2 = 4(\delta D_1 - \delta D_2)^2 + (\delta P_1 - \delta P_2)^2 + (\delta H_1 - \delta H_2)^2$. The smaller the R_a, the more likely they are to be compatible.[120]

Table 2 Comparison of 0D, 1D, and 2D materials in their bio-interfacing properties

Dimensional architecture	0D 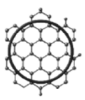	1D 	2D 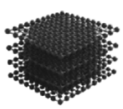	3D 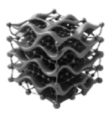	Ref.
Quantum confinement	Spherical; better quantum confinement with discrete energy levels	Elongated nanowire; one-dimensional confinement	Planar layered nanosheets; quantum confined in the *x*–*y* plane only	Minimal quantum confinement: delocalization of electrons across all dimensions	101–104
Bio-interfacing	Internalization *via* endocytosis	Interactive along length	Continuous membrane interfacing	Scaffold biomimetic matrix	105–108
Surface contact	Isotropic-high reactivity	Anisotropic-high reactivity	Large interfacing-high surface reactivity	High surface contact	109–111
Morphology driven functionality	Small size-uniform surface coating	Cylindrical interface-directional coating	Planar interface-multivalent functionalization	Structural support-3D tissue integration	112–114
Translational challenges	High agglomeration, cytotoxicity	Low degradation, high rigidity	Poor scalable synthesis, oxidative, reduced stability	Complex architecture, limited control on nanoscale synthesis	115 and 116
Biomedical systems	Cellular tracking, diagnostics and sensing, drug and gene delivery	Wearable electronics, sensing and diagnostics, antimicrobial applications	Wearable electronics, therapeutic diagnostics and sensing, cellular therapies	Tissue engineering, organ on chip, bone and cartilage substitutes	106, 107, 111, 114 and 117

Table 3 HSP of biomolecules and 2D materials

	δD $(MPa)^{1/2}$	δP $(MPa)^{1/2}$	δH $(MPa)^{1/2}$	Δt $(MPa)^{1/2}$	Ref.
Proteins (BSA[a])	19.9	18.2	17.5	32.1	118
DNA	19	20	11	29.70	120
Lipids (POPC[b])	16.10	6.40	9.10	19.56	121
Graphene	18.001	9.30	7.70	21.67	122
MoS_2	17–19	6–12	4.5–8.5	18.5–24	123
$Ti_3C_2T_x$	18.71	15.4	14.5	28.2	124
RGO	17.5	9.5	14.4	24.6	125
MWCNTs	16.8	2.4	13.9	12.2	118
BNNTS	16.8	10.7	14.7	24.75	126

[a] BSA: bovine serum albumin. [b] POPC: phosphatidylcholine.

As shown in Table 3, MXene exhibits a significantly higher polar component compared to other nanomaterials. This increase can be attributed to the surface-terminated functional groups, such as =O, –OH, and –F, obtained from the aqueous etching synthesis process. Large electronic groups contribute to strong polar interactions in the clustered phase of MXene. Additionally, high values of δD and δH indicate considerably high dispersive and hydrogen bonding interactions among MXene layered structures.[124] These properties significantly influence the surface interactions with biomolecules, as discussed later.

Lipids. As presented in Table 4, the degree of compatibility generally for most 2D materials with biomolecules follows the rule lipids > DNA > proteins, with lipids demonstrating the strongest interaction. Such high compatibility can be attributed to the close match between the C–C–C bond distance along lipid alkyl chains (2.56 Å) and the hexagonal lattice spacing in these materials (2.46 Å), allowing lipids to adopt a lying-down orientation on 2D material surfaces, enabling strong adsorption.[127]

An interesting observation from the R_a values in Table 4 is that multi-walled carbon nanotubes (MWCNTs) exhibit a lower affinity for all biomolecules in general when compared to graphene. It is indeed found (Fig. 4) that the curvature of carbon nanostructures significantly affects the R-helix structure of the adsorbed proteins.[91] In contrast, the van der Waals interaction between the 2D materials' surface and peptides becomes more favorable upon decreasing the curvature. This underscores another unique aspect of 2D materials in studying interactions with biomolecules and the design of hybrid biomolecular devices.

The lipids' arrangement on 2D materials is dependent on their functional groups. For instance, alkanes form striped lamellar phases, with the stripe width influenced by the chain length. Lipids with small functional groups, such as hydroxyl (–OH), tend to align perpendicularly to the substrate, while those with larger headgroups, such as carboxyl (–COOH), lie parallel to the surface.[127] Also, hydrogen bonding between headgroups can alter lipid assemblies' orientation and domain structure. Phospholipids and long-chain carboxylic acids often assemble into ordered striped phases on 2D materials when deposited using techniques like Langmuir–Schaefer transfer.[127]

For instance, graphene interacts with phospholipids through a collective movement dominated by van der Waals forces. The interaction becomes hydrophobic once the initial attraction occurs, particularly between the graphene surface and the lipid tails. This affinity is largely due to the alignment of the alkyl chains of lipids with the hexagonal lattice of graphene, making lipids more compatible with graphene compared to other biomolecules like DNA and proteins.[128]

On the other hand, graphene oxide (GO) shows a different interaction pattern due to its oxygen-containing functional groups, which reduce van der Waals forces by introducing polarity. GO's interaction with lipids varies according to the degree of oxidation and lipid phase. GO can either insert obliquely into lipid bilayers or become sandwiched between leaflets, depending on its oxidation level and the type of lipid membrane. In the case of 1,2-dioleoyl-*sn-glycero*-3-phosphocholine (DOPC) bilayers, GO inserts at a 25% oxidation level, while in dipalmitoyl phosphatidylcholine (DPPC) bilayers, it may detach from the membrane surface at higher oxidation levels.[129]

MXenes, such as $Ti_3C_2T_x$, present a lower affinity for lipids than graphene and GO due to their higher polarity and hydrophilicity. Although MXenes can infiltrate lipid membranes, the process typically requires external force and occurs less spontaneously than in the case of graphene-based materials. Unlike graphene, MXene demonstrates less spontaneous lipid interaction, particularly due to its polar surface chemistry.[130]

Nucleic acids. Nucleic acids, particularly DNA, demonstrate a notable affinity for 2D materials, ranking just below lipids regarding compatibility with such surfaces (Table 2). While it might initially seem unusual for DNA to have an affinity for 2D materials due to its highly charged phosphate backbone, the hydrophobic base pairs within DNA primarily drive this interaction. The HSP values for DNA, dominated by its bases, are approximately [19.8, 12.3, 12.2] (Table 3), suggesting that despite the hydrophilic ribose-phosphate backbone, the core of DNA is relatively compatible with 2D materials.[120] This makes DNA also a favored biomolecule for interactions with such materials.

For most 2D materials like graphene, DNA typically adsorbs *via* π–π stacking and hydrogen bonding interactions, particularly between the base pairs and the material's surface. However, MXenes exhibit a different behavior. Instead of relying on π–π stacking or hydrogen bonding, MXenes like $Ti_3C_2T_x$ primarily interact with DNA through electrostatic interactions. Interestingly, MXenes demonstrated the highest compatibility with DNA, reflected in the smallest R_a value (Table 4). This is unexpected since DNA and MXenes carry strong negative charges, meaning that significant electrostatic repulsion must be overcome for DNA adsorption.

In previous studies, Mn^{2+} ions were shown to neutralize the DNA phosphate backbone, facilitating oligonucleotide adsorption

Table 4 R_a values between biomolecules, 2D materials, and nanotubes

	Proteins (BSA)	DNA	Lipids (POPC)
Graphene	13.77	11.37	4.98
MoS_2	18.75–11.08	15.95–8.38	4.96–8.08
$Ti_3C_2T_x$	4.75	5.81	11.71
RGO	10.41	11.44	6.75
MWCNTs	17.35	18.37	6.44
BNNTs	10.13	10.93	7.20

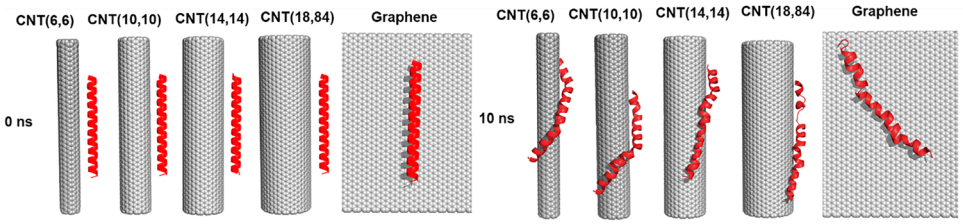

Fig. 4 The influence of surface curvature on the strength of peptide interactions, adapted from ref. 91 (Copyright 2011 *J. Phys. Chem. C*).

onto MXene.[15] Another study hypothesized that the negatively charged MXene surfaces (−30 mV) form ion bridges with DNA, accounting for their interactions.[131] However, both studies agree that the surface interaction remains weak, indicating that further research is needed to understand the underlying mechanism of DNA–MXene interactions fully.

Peptides. Although proteins rank third in affinity for 2D materials (Table 2), they have been extensively studied for surface patterning and functionalization. These biomolecules primarily interact with 2D materials through π–π stacking between their aromatic groups and the 2D surface.[132] The formation of monolayers on these surfaces is influenced by the arrangement of these aromatic groups, promoting non-covalent interactions that help stabilize the binding. However, the relatively low affinity of proteins for 2D materials often leads to significant protein unfolding and deformation. This structural change exposes hydrophobic regions of the protein, affecting its stability and final conformation on the graphene surface.[132] The low affinity explains the inevitable denaturation and conformational changes in proteins bound to 2D materials such as graphene and MoS_2, highlighting the challenges in maintaining their functional integrity.

The significance of aromaticity and amphiphilicity was further demonstrated in a study that mutated the GrBP5 peptide sequence to create three variants: one lacking an aromatic ring and two with different arrangements of aromatic residues, leading to varying amphiphilic profiles. The non-aromatic variant exhibited no peptide adsorption, underscoring the critical role of aromatic residues in interactions with graphene surfaces. The two aromatic variants displayed distinct structural outcomes; the variant with higher amphiphilicity formed a porous, ordered peptide network, while the other produced small, isolated peptide islands.[132]

A similar trend was observed with hexagonal boron nitride (h-BN), where peptides enriched with histidine and tyrosine (Tyr) residues exhibited a high affinity for the material. This affinity is unsurprising, as the BN structure allows for complementary π–π interactions. Further studies on h-BN revealed that mutating the aromatic Tyr residue (Y8A) decreased fluorescence by 90%, indicating that similar π–π interactions, as seen with graphene, are also significant in the case of BN.

While aromaticity is a key factor in peptide and protein interactions with 2D materials due to electron donation from amino groups to the π-system of nanosheets, other forces contributed by amino acids also play a crucial role in determining the overall strength and extent of these interactions. Hydrophobic interactions, influenced by amino acids such as Ala, Pro, Leu, and Met, depend on electron density and molecular geometry. Additionally, electrostatic interactions involving amino acids like Lys, Arg, Glu, and Asp are influenced by the charge of surface-functionalized groups on the nanomaterial and the charge of the amino acids, where zeta potential values can serve as indicators of binding efficiency, sensitive to the pH of the medium and the ionic strength of the buffer.[133]

In contrast to many other 2D materials, MXenes possess excellent hydrophilicity due to their abundant surface-terminating groups. This hydrophilic nature and multiple hydrogen bonds are essential for their interaction with proteins, allowing them to retain a higher degree of their original structure without undergoing deformation.[134]

3.3 Time scale of interaction

When 2D materials interact with a biological environment, they acquire a new "biological identity" as multiple layers of biomolecules, such as proteins, lipids, DNA, and RNA, accumulate on their surface. This transformation is driven by the material's preferential interactions with specific biological components. Several molecular analysis studies have demonstrated this effect, where liquid-phase exfoliation has been used to prepare nanosheets in the presence of biomolecules. This leads to distinct profiles of the biological corona surrounding the 2D material based on preferential interactions.[135]

The nanomaterial-associated biological corona depends on several variables, including the biological medium and the physicochemical characteristics of the nanomaterial, which can alter the nanomaterial's biodistribution, clearance, activity, and toxicity by modifying its hydrodynamic size, shape, charge, and interfacial properties.[136] This affects the rational process of designing 2D material bioconjugate devices/systems.

One of the studies examined the protein profile of graphene exposed to biological media and resolved the composition through proteomic analysis.[135] Using human serum at various concentrations, the findings revealed that graphene acquired a new protein identity, particularly enriched in apolipoprotein A–I. For example, for possible identification of the biological identity of the graphene nanoflakes, protein layer orientation was investigated using proteomic analysis. The graphene nanoflakes were exfoliated under varying human serum concentrations (HS). The statistical distribution in the pie chart (Fig. 5) showed that the strongest binding affinity was obtained for lipoproteins, immunoglobulins, and high-density lipoprotein (HDL). Interestingly, apolipoprotein A–I, the major component

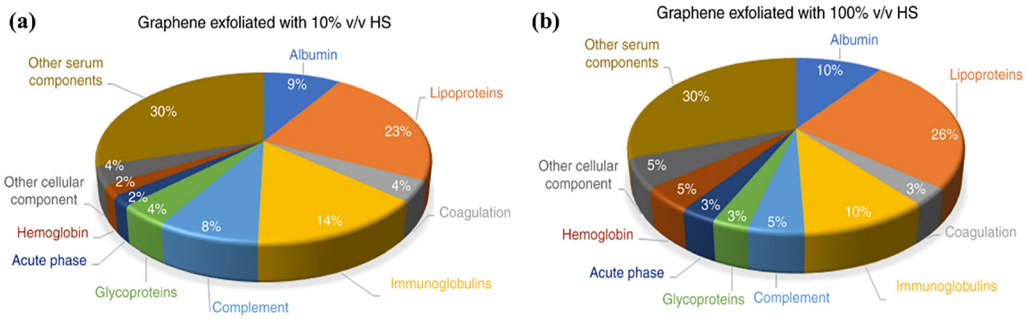

Fig. 5 Pie charts (a) and (b) indicating the relative coverage of protein, as identified by mass spectrometry, onto the graphene flakes exfoliated with 10% v/v and 100% v/v of HS, respectively.[137] (copyright 2018 *Nature*).

of HDL, was highly abundant on the nanoflakes exfoliated with HS. This high distribution of HDL suggested that the self-organization of the supported lipid bilayer on GO flat surface nanoflakes most probably occurred because of the strong interactive capability of the GO surface with phospholipids.[137]

Further research explored the lipid profiles of few-layer graphene (FLG) and graphene oxide (GO), revealing differences in how the bio-corona forms around these materials in human plasma. For example, the lipid lyso-PE 20:4, commonly found in plasma, was present in the corona surrounding FLG but was minimally represented in GO's corona. Conversely, certain lipids, such as PS 38:4, were enriched in the corona of both FLG and GO compared to their native abundance in plasma, indicating a stronger affinity for these lipids in the interaction with graphene-based materials.[138]

In both scenarios, the nanosheets interacted with most of the biomolecules in the medium to a certain extent, with different percentage coverage reflecting the presence of two main interfaces: a loose interface characterized by distinct particles and a tight interface with molecules more strongly associated with the surface. The loose interface can arise due to the selectivity of the 2D material's surface when exposed to a mixture of biological elements, or it can form as a second layer interacting with the biological elements already on the 2D material's surface. This concept can be compared and extended to the formation of soft and hard corona layers when introducing a foreign object or nanoparticle into the body.[139]

A useful theoretical analogy for understanding such layered organization is provided by the Gibbs dividing surface. The Gibbs dividing surface is an imaginary boundary between two phases. It is not a physical surface but a mathematical construct used to define and calculate interfacial properties such as surface tension, adsorption, and excess quantities, with the choice of dividing surface being somewhat arbitrary. By analogy, this concept can be extended to biological systems, where in Fig. 6 a boundary recognition dividing surface may be considered as the intermediate layer at which functional recognition and information exchange occur with the biological molecule.[140]

It is important to note that the formation of these layers in association with the 2D material is more related to the timescale of events that lead to the more favorable or least favorable interaction, regardless of the specific origin of the biomolecular species. Therefore, for instance, the tighter layer could be formed due to variations in proximity from the nanostructure or the availability of certain biomolecules more than others.[141]

Molecules that lie above the boundaries in Fig. 6 move (relax) more slowly than the recognition time (of the molecule by the 2D material), and those lying on the other side relax faster than this. Therefore, the challenge in revealing the nanostructure's biological identity lies in capturing and analyzing such a surface,[139] especially in surfaces with a constant shift between entrapment and release of biomolecules, as shown in ref. 131.

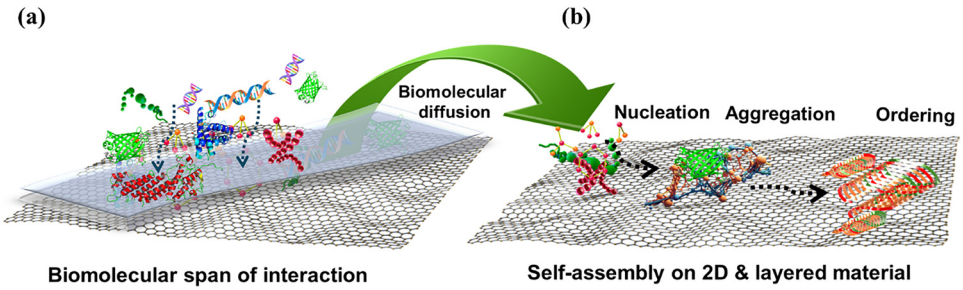

Fig. 6 (a) Biomolecules close to the nanosheets exhibit slower movement, while those farther away relax more quickly, with a grey surface indicating the boundary between these regions. (b) After successful interaction with the nanosheet, biomolecules undergo (i) nucleation, (ii) aggregation, and (iii) ordering, which is influenced by the density of biomolecules on the surface (created in **https://BioRender.com** and **https://BioRender.com** and **https://www.freepik.com**).

In a mixture also, the favorable interaction between the biomolecules themselves and the environment should be considered; in more complex systems, where loosely bound molecules on the surface of the nanostructure, being less engaged, are squeezed out, only the nanostructure itself and molecules most strongly associated with it are finally recognized.[142,143]

3.4 Span of interaction

All biological fluids are multiprotein systems; various proteins compete with each other and with other surface-active components for adsorption at any interface present. As a rule, the sorbent surface will at first become covered by the molecules with the highest arrival rate, *i.e.*, the smaller ones with the highest diffusion coefficient and the ones that occur most abundantly in the solution.[144] At later stages, the initially adsorbed molecules may be displaced in favor of other molecules with a higher affinity for the surface. Competitive adsorption between monomers, dimers, or higher aggregates of the same type of protein is easily understood in terms of more anchoring segments per adsorbing entity as the number of segments in that entity increases.[144] Thus, preferential adsorption of aggregates, relative to monomers, has been reported; *e.g.*, in a serum albumin study, lipoproteins had the highest percentage of interaction with graphene compared to other proteins. The time scale and span of interaction control the structural heterogeneity of biomolecules in the adsorbed layer, which depends on the rate of attachment and spreading relative to each other. When spreading occurs relatively quickly, the adsorbed molecules are more flattened. If the protein flux to the surface increases, the adsorbed molecules retain a more globular conformation and, therefore, the adsorbed mass per unit surface area is higher.[144]

Similarly, molecules arriving at an early stage of the adsorption process find sufficient area available for spreading, whereas this is not the case for the molecules that arrive when the surface is already (partially) covered. This is governed by the biomolecule's interaction and adsorption, which comprise various aspects, including kinetics, type of binding, and adsorption. Once the molecule has attached, it relaxes toward its equilibrium structure, which, because of the altered environment, differs from the (native) structure in the solution.[144] Structural relaxation occurs when a larger number of molecule-surface contacts develop. Consequently, it becomes more difficult for the protein to detach from the surface after relaxation. It is important to note that relaxation becomes more difficult as the interaction between the molecules and 2D materials is stronger because nonequilibrium states tend to become quenched (not flat/unstable).[144]

4. Design criteria for 2D material-based bio integrated devices for targeted interactions

When designing systems that integrate 2D materials with biomolecules, it is crucial to account for the mutual effects they exert on each other as well as the targeted biological applications. For example, when the primary objective is to preserve the biomolecule's properties, appropriate functionalization and surface modification of the 2D material may be necessary to avoid deformation, denaturation, or changes in the biomolecule's conformation. For applications where maintaining specific orientations of biological moieties is essential, customized surface functionalization is required to preserve the desired positioning. When it comes to system-level interactions mainly for translational application scenarios, then other parameters need to be considered and accounted for in the material design and functionalization.

4.1 Intrinsic material properties

Intrinsic properties of 2D materials, such as conductivity, can be leveraged to control the interaction patterns between 2D materials and biomolecules based on specific requirements. For instance, in a former study[145] the authors applied voltage to modulate the nucleation sites of peptides on graphene surfaces, demonstrating how graphene's high conductivity allows changes in the reaction potential to influence bioconjugate structures significantly. In binding experiments at a concentration of 1.0 μM within a potential range of −1 to 0.5 V, notable changes in peptide surface morphology were observed *via* AFM imaging. GrBP5 peptides formed dendritic-like surface patterns at negative potentials, while at 0 V, the adsorbed peptides exhibited linear or wire-like morphologies. As the voltage increased to +0.5 V, the linear structures became more curved, forming wave-like patterns. These morphological transformations illustrate the influence of system potential on bioconjugate formation.

4.2 Structural defects

Structural defects of 2D materials play a crucial role in device design. For example, MoS_2 nanosheets have been shown to interact with polyaniline, disrupting its intramolecular hydrogen bonding and inducing significant conformational changes that alter the polymer's secondary structure. Defective MoS_2 nanosheets typically exhibit porous structures essential for single protein sequencing. Chen *et al.* investigated protein translocation through MoS_2 nanopores using molecular dynamics simulations, revealing that the interactions between peptides and defective MoS_2 nanosheets were predominantly governed by van der Waals interactions.[13] A combination of *in silico* and *in vitro* analyses could also be helpful for the in-depth evaluation of possible binding parameters of 2D materials and surface proteins; for example, molecular docking combined with *in vitro* analysis (Vero E6 cell cultures) identified the binding parameters of GO with SARS-CoV-2 viral components.[146] These molecular docking data showed enhanced binding affinity of GO to the viral spike proteins and ACE2 cell receptors. GO caused pronounced viral inhibition, and is a promising candidate for antiviral therapeutic purposes.[146] The effect of defects was also demonstrated in a comparative study,[147] which investigated both defective graphene (D-Gra) and pristine graphene (P-Gra). It was shown that both can attract double-stranded DNA (dsDNA) to form stable bindings. However, the structural evolution of dsDNA differs significantly

between the two materials. Specifically, D-Gra can rapidly unwind dsDNA and cause substantial structural disruption, while P-Gra exhibits a weaker capacity to disrupt the dsDNA structure. This difference arises from the strong electrostatic interactions between defects in D-Gra and DNA nucleotides. The defects tightly constrain the nucleotides, allowing other parts of the dsDNA to move laterally along D-Gra. This effectively introduces a "pulling force" from the defects that breaks the hydrogen bonds between dsDNA base pairs, ultimately leading to significant unwinding of the dsDNA.[147,148]

The P1 peptide, composed of histidine and arginine residues, has been reported to promote non-covalent functionalization of graphene without significantly altering its electronic properties.[70] Studies have shown that P1 preferentially binds to the basal plane of graphite, enabling the exfoliation of few-layer graphene with relatively low defect densities. Due to the absence of additional functional domains, P1 tends to yield higher-quality graphene compared to multidomain peptides, as it introduces fewer lattice disruptions during exfoliation.

Doping enables fine-tuning of the molecular configuration of a material, making it possible to control surface adsorption predictably. Such modifications facilitate the design of bifunctional materials for applications like biosensing and drug delivery. Not only do these modifications have the potential to alter adsorption patterns, but they also influence the areas of the coating, such as the basal plane, edge interactions, and defect sites. This behavior can be utilized to map the surface properties of 2D materials by studying the functionalization positions.

4.3 Surface functionalization

The chemical functionalization of 2D and layered material surfaces, such as covalent binding (101), covalent grafting, π–π stacking,[149] van der Waals interactions, non-covalent adsorption,[150] biomolecular self-assembly annealing,[151] thermal decomposition, and oxygen or argon treatments,[152] is used for inducing localized functionalization or surface patterning (Fig. 7(a)).[153]

Controlled functionalization allows the patterning of graphene films as flexible, transparent electrodes for displays and touch screens.[154] Hydrogen bonding, π–π stacking, metal–ligand coordination, and charge-transfer cellular interactions drive the diversity of interactions in biomolecular self-assembly. The covalent functionalization of graphene involves the rehybridization of sp^2 carbons to sp^3, altering graphene's electronic properties through hydrogenation, fluorination, radical additions, cycloadditions, and oxidation. On the other hand, non-covalent functionalization through π–π stacking with aromatic molecules preserves graphene's electronic structure. The chemical doping or surface treatments can modulate a zero-gap semimetal to a p-type or n-type semiconductor (hydrogenated graphene) or into an insulator (fluorinated graphene). Physisorption of solution-processed transition metal dichalcogenides (such as MoS_2, WS_2), covalent modification (with alkyl halides, aryl diazonium salts), and coordinative bonding (*via* metal complexation) can tailor the bandgap transitioning properties, catalytic activity, and sensing capabilities.[155] The non-covalent functionalization approaches like van der Waals forces and Lewis acid–base complexation are preferable because of minimal structural damage, good dispersibility, high mechanical strength, and procesibilty.[150]

However, bio-functionalization is highly effective for introducing surface versatility while preserving the intrinsic characteristics of the 2D materials, which improves their integration into bioelectronics. For example, graphene flake surfaces (zeta potential approx., +35.4 mV) are biofunctionalized with hydrophobic protein coatings for promoting the electrostatic interaction with the negatively charged 2D layered materials such as MoS_2 flakes (−22.5 mV). These bio-functionalization approaches lead to van der Waals coupling mechanisms, stabilized dispersions, reduced electronic structure disruption, and enhanced non-covalent conjugation with other biomolecules like antibodies and enzymes.[151] The proper solvent selection is also crucial for improved surface reaction kinetics, stable suspensions and removal of unreacted byproducts for good conjugations at bio interfaces.[156] Photochemical effects from laser irradiation introduce high-energy defects into confined spaces on TMDs and GO for patterned functionalization. High-energy beam exposure results in thermal carbonization of the carbon-containing material, which introduces abundant oxygen, hydroxyl, and carboxyl functional groups on the material surface and edge sites.[157]

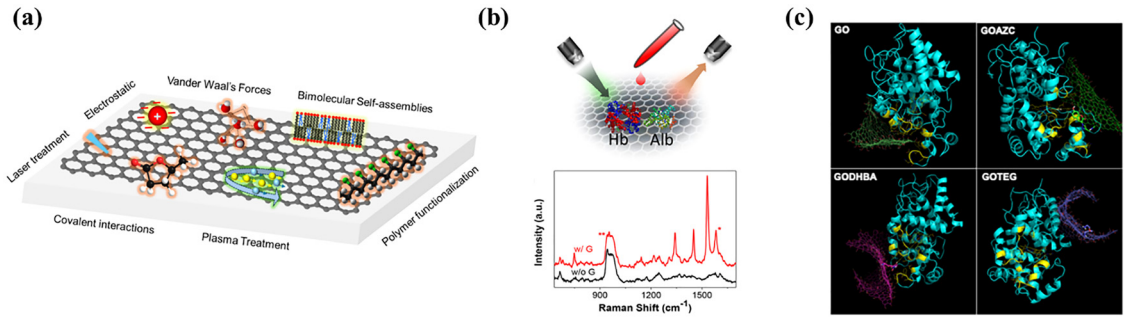

Fig. 7 (a) A simplistic schematic representation of 2D and layered materials' surface functionalization approaches (created in https://BioRender.com and https://www.freepik.com). (b) Graphene-enhanced Raman scattering (GERS) approach for signal enhancement upon biomolecule interaction with graphene[158] (copyright, 2018 *ACS Photonics*). (c) Molecular modeling showing possible binding between horseradish peroxidase and GO[159] (copyright 2018 *2D Mater.*).

Selective and reproducible Raman signal amplification can be acquired when biomacromolecules are in contact with graphene (Fig. 7(b)) because of high charge transfer and π–π interactions between the graphene surface and biomolecules. This label-free approach provided molecular fingerprint information, for the future differentiation of biomolecules based on their structure and oxidation states.[158] The horseradish peroxidase functionalization enables the binding of ligand molecules, *i.e.*, 7-hydroxy azido coumarin (AZC) and 3,4-dihydroxybenzoic acid (DHBA), to the active sites of GO, enhancing electron transfer and promoting complete biodegradation. Furthermore, the negative surface charge of GO facilitates enzyme binding by attracting positively charged domains of proteins through electrostatic interactions and by preventing sheet aggregation, which maintains a larger exposed surface area. These combined effects enhance enzymatic degradation and could reduce the persistence of GO in biological systems (Fig. 7(c)).[159] Additionally, surface functionalization of materials with a polymer matrix reduces their surface energy and improves their dispersion, stability and effectiveness in biological system applications.[160]

4.4 System-level interactions and device engineering towards *in vivo* applications

System-level interactions of 2D materials encompass their dynamic behavior within the complex milieu of living organisms, extending beyond local cellular effects as described above, to organ systems to whole-body responses. Key considerations include immune recognition, biodistribution, and clearance pathways, as well as their ability to cross biological barriers (see Section 5) and maintain biocompatibility over time. Successful bio-integration is hindered by persistent challenges such as oxidative stress, tissue inflammation, antimicrobial resistance, and cytotoxicity. Surface functional groups including hydroxyl, epoxy, and oxidized states can exacerbate membrane damage and compromise cellular viability, amplifying inflammatory cascades. Thus, engineering strategies must move beyond material design alone to actively regulate biological responses. Together, understanding and harnessing system-level interactions between 2D materials and the biological environment in conjunction with device and material engineering is critical for device stability, therapeutic efficacy and long-term safety toward translating 2D materials into viable *in vivo* bioelectronic and biomedical applications (Fig. 8).

Effect of biomolecular interactions. For biomolecules, particularly peptides, aromatic groups confer strong binding to graphene surfaces but can induce conformational changes or denaturation. Preserving the native protein structure may require mutating specific residues or altering amino acid sequences to reduce π–π interactions between aromatic side chains and graphene This can be achieved by substituting alanine for two hydrophilic residues (Gln32 and Asn35) or grafting aromatic groups onto the outer structures of biomolecules to minimize unfolding[132] and ensure optimal association with the surface.

The bioconjugation process can significantly impact semiconducting behavior, electrical performance, and mechanical

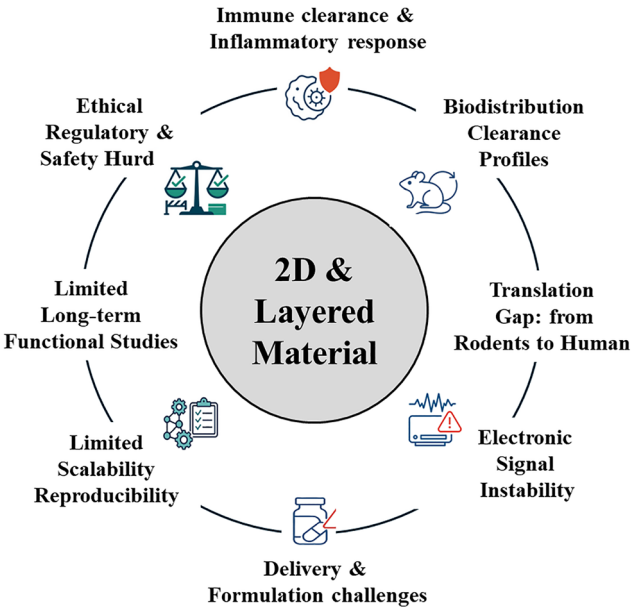

Fig. 8 Schematic illustration highlighting the current translational limitations identified in recent *in vivo* studies on 2D material bio interfaces.

characteristics of 2D materials; in a study investigating the interaction between 2D materials and oligoglycine tectomers,[161] it was demonstrated that the bio-layer formed from interacting amino acids affected the doping mode of the materials depending on the number of layers. Single-layer MoS_2 exhibited p-doping accompanied by tensile strain, while multilayer MoS_2 displayed n-doping associated with compressive strain. In contrast, graphene consistently remained n-doped due to the amine groups of the tectomers, regardless of the number of layers, and no significant additional strain was observed in either single- or double-layer graphene. This stability enables effective modulation of the Fermi level, which is advantageous for sensing applications.

Additionally, the interaction of biomolecules with graphene and MoS_2 was shown to induce localized mechanical strain (π) and alter charge carrier density (n) compared to their pristine states, resulting from ambipolar charge transfer from amino acid groups. These differences underscore the importance of selecting the appropriate 2D material based on the desired biomolecular interaction and specific application. Additionally, the concept of utilizing significant areal doping presents opportunities to interface with other 2D nanomaterials, enabling the fabrication of novel layered composite materials.[162]

Understanding and predicting interactions with the immune system. The interaction with the immune system is a crucial and foundational aspect in developing any biological interface involving advanced materials. In the context of graphene and other carbon nanomaterials, the nanoimmunity-by-design concept was recently proposed due to two multidisciplinary projects funded by the European Commission, G-IMMUNOMICS and CARBO-Immap.[163]

Nanoimmunity-by-design involves detailed characterization, considering not only the physicochemical properties of the materials but also their immunological characteristics. These

immunological properties can result in either immune activation or suppression, both of which have valuable applications for several biomedical devices (Fig. 9). Nanoimmunity-by-design could enable the classification of materials based on their immunological profiles introducing a technological pipeline and a computational modeling framework capable of predicting material behavior in biological fluids and their interactions with cells.

By leveraging high-throughput methods such as proteomics and genomics for functional characterization, it is possible to generate extensive datasets for 2D materials that require systematic integration. Aligning these data with molecular patterns associated with human diseases, drug treatments, and chemical exposures allows the positioning of nanomaterials within these contexts. Such systematic relationships can help identify adverse outcome pathways or mechanisms of action, potentially facilitating their device' application. By incorporating the nanoimmunity-by-design concept, nanomaterials can be engineered with consideration of their potential applications, offering a groundbreaking perspective on the design and safe deployment of graphene-based materials and other carbon-based nanomaterials.

Efforts to elucidate the immunological properties of graphene-based materials and other carbon-based nanomaterials have leveraged advanced high-throughput techniques to characterize their interactions with the immune system. Central to this approach is the concept of intentionally designing nanomaterials with tailored immune modulation properties. This represents a paradigm shift in nanotechnology and materials science, focusing on the physicochemical attributes of nanomaterials and their biological and immunological profiles.[164] Graphene-based materials in different EU-funded projects (Graphene Flagship, G Immunomics, CarboIMMAP, and MX-MAP) have been investigated using state-of-the-art techniques such as single-cell mass cytometry and transcriptomics, enabling an unprecedented level of precision in immune profiling.[163] Their effects have been assessed across various experimental models, including human cells, animal systems such as *Sus scrofa* (swine)[165] and *Mus musculus* (mice), *C. elegans*, and *ex vivo* systems.[166] This multidisciplinary approach has provided a comprehensive understanding of how these materials interact with the immune system. One notable finding is the selective cytotoxicity of few-layer graphene against malignant monocytes. This property positions few-layer graphene as a promising candidate for cancer therapy, with the ability to selectively target and eliminate tumor cells while sparing healthy ones. Experimental evidence demonstrated that few-layer graphene induces necrosis in monocytes derived from patients with myelomonocytic leukemia without affecting other immune cell types.[167]

This finding underscores the potential of graphene-based materials as anti-cancer devices.

Further research incorporated computational models to map the immune activity of carbon-based nanomaterials. This approach aimed to establish correlations between the physicochemical properties of nanomaterials and their biological effects, facilitating the predictive design of materials with tailored immune properties. Among the carbon-based nanomaterials, functionalized nanodiamonds exhibited distinct immunological impacts depending on their surface chemistry. For example, nanodiamonds functionalized with carboxylic acid groups elicited a more pronounced pro-inflammatory

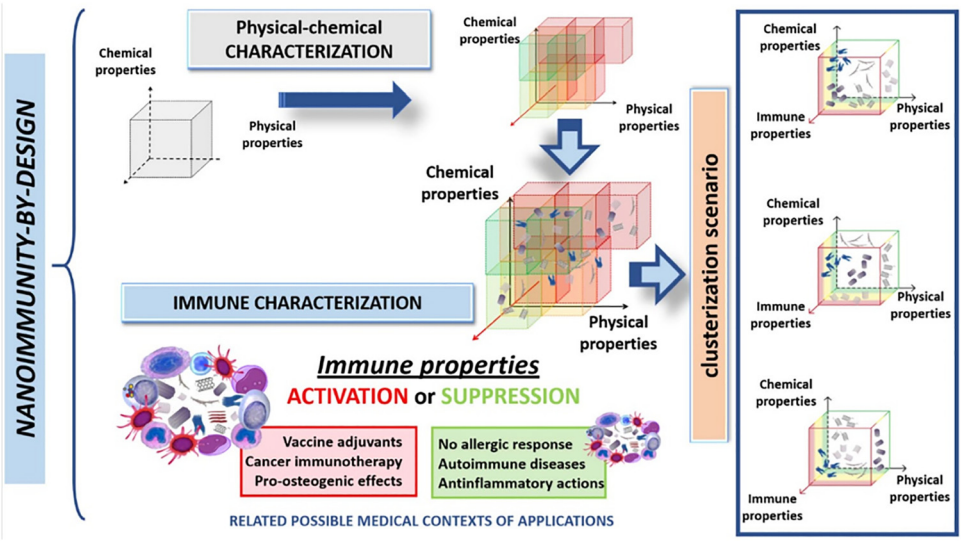

Fig. 9 Graphical representation of the nanoimmunity-by-design concept. The design of nanomaterials requires an in-depth characterization process based not only on the physicochemical properties of the materials (upper part) but also on the analysis of their immunological properties (middle part). The different immune properties may lead to immune activation or suppression, both potentially useful in various biomedical contexts (bottom part). By combining the immune properties with the material physicochemical properties, clusterization of the nanomaterials can be obtained to serve as a platform for future modeling and systems biology-based approaches. Adapted from DOI 10.1088/2515-7639/ab9317 2020 *J. Phys. Mater.*, under the terms of the Creative Commons Attribution 4.0 License.[163]

response compared to those functionalized with amino groups, which were better tolerated by immune cells.[168] Beyond graphene-based materials and nanodiamonds, carbon nanotube fibers have also been explored for their potential as conductive materials in biomedical applications. Their unique electrical and mechanical properties make them suitable for use in biosensors, neural interfaces, and tissue engineering scaffolds. Understanding their interactions with biological systems is essential for optimizing their performance and ensuring their biocompatibility, ultimately expanding their potential applications in healthcare and beyond. Carbon nanotube fibers have been explored as sutures for myocardial repair, utilizing their excellent conductivity to help restore electrical conduction in damaged heart tissue. Experiments in animal models demonstrated that carbon nanotube fibers could maintain myocardial conduction without eliciting significant immune or inflammatory responses, highlighting their potential as a biocompatible tool in cardiac medicine.[169]

The concept of nanoimmunity-by-design provides a framework for tailoring nanomaterials to specific therapeutic goals, whether by inducing immune activation for cancer treatment or promoting immunosuppression to mitigate inflammation and autoimmune disorders. Integrating high-throughput screening techniques with computational modeling accelerates the development of safe and effective nanomaterials for clinical applications. It also provides essential data to guide regulatory standards for their production and use. This knowledge helps inform the intentional design of nanomaterials with tailored properties, ensuring their compatibility with biological systems and interfacing for creating new effective devices.[163] As the field continues to evolve, the principles of nanoimmunity-by-design will undoubtedly play a pivotal role in shaping the future of 2D material biomedical devices.

Controlling cytotoxicity and cellular uptake. Recent studies highlight the promise of engineering surface chemistry, dimensional stability, and stimuli responsiveness to modulate bio–nano interactions effectively thereby controlling cytotoxicity and cellular uptake. For instance, integrated stimuli-responsive MOF hydrogels in rats and rabbits actively regulate immune responses by releasing gallic acid and Mg^{2+} ions under acidic stress, thereby suppressing ROS and cytokine production, while simultaneously promoting angiogenesis and osteogenesis.[170] $Ti_3C_2T_x$ MXene (Fig. 10(a)) demonstrates excellent biosafety as a photothermal neural transducer, enabling repeatable modulation with ultra-low-energy pulses (<10 μJ, up to 10 Hz) without mitochondrial damage.[171] Similarly, MXene-incorporated PMMA/PDMS nanofibers enhance viability, mechanical stability, and radiopacity, supporting long-term vascular graft applications.[172] Other works include quaternary pullulan-MoS_2 coatings achieving >99.5% antibacterial efficacy with minimal inflammation,[173] while Mg-Dex/BP/PLGA implants (Fig. 10(b)) promote osteogenesis but suffer from rapid BP degradation leading to Mg corrosion and

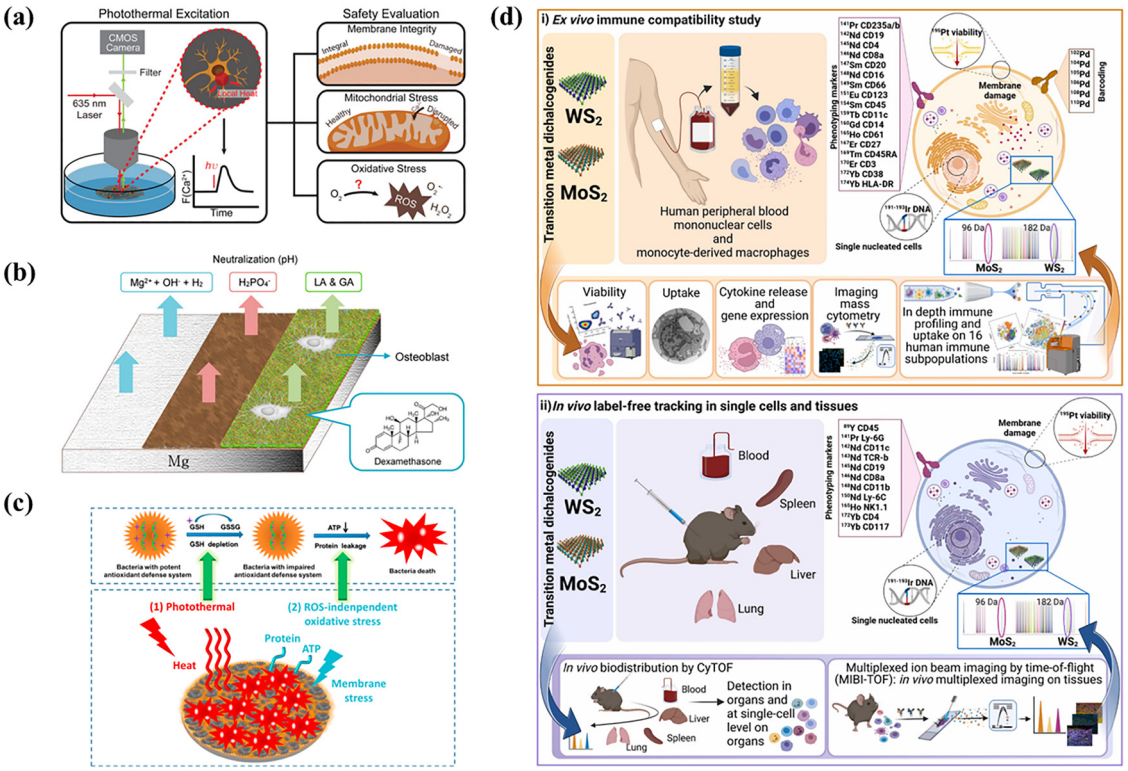

Fig. 10 (a) Schematics for safety evaluation assessment of photothermal excitation of neurons including membrane integrity, mitochondrial stress, and ROS generation.[171] (b) Mg substrate surface-modified with dexamethasone-loaded BP and PLGA to facilitate osseointegration.[174] (c) Schematic illustration of the antibacterial mechanism of MoS_2/PDA-RGD coating: the photo-thermal effect and ROS synergistically caused a distinctive lethal effect on bacteria.[175] (d) Schematic representation of MoS_2 and WS_2 detection in cells and tissues using mass cytometry-based detection.[177]

tissue necrosis.[174] MoS_2/PDA-RGD dental coatings (Fig. 10(c)) achieve 94.6% antibacterial efficiency under NIR, mimicking bone environments to enhance osseointegration and wound healing.[175] Meanwhile, TiS_2 coatings inhibit Candida biofilms but impair gingival fibroblast growth.[176] Advanced immune profiling *via* CyTOF (Fig. 10(d)) revealed that MoS_2 and WS_2 nanosheets outperform graphene in biocompatibility and biodistribution, supporting their promise as non-destructive, label-free biomedical alternatives.[177]

Understanding and controlling protein corona. Identifying distinct ''safe'' and ''toxic'' protein corona profiles offers a pathway for the rational design of 2D materials and could accelerate their clinical translation in bio-integrated devices. As discussed earlier, the tunable surfaces of 2D materials provide an advantageous platform for probing protein corona formation on both bare and functionalized interfaces. Molecular dynamics simulations indicate that proteins bind to graphene oxide (GO) primarily *via* π–π stacking and hydrogen bonding, with aromatic tyrosine and positively charged arginine and lysine residues playing key roles.[178]

Surface engineering can markedly alter these interactions. Introducing hydrophobic functional groups such as azide or alkyne to the GO surface creates steric hindrance, limiting protein and water access to oxygen-containing groups on the basal plane and edges. This modification significantly reduces protein adsorption: from 1.4 mg for unmodified GO to 1.1 mg for partially modified GO (22% reduction), 0.9 mg for azide-modified GO (GO–N_3, 35% reduction), and 0.8 mg for alkynylated GO (C_2GO, 43% reduction). The diminished protein coating correlated strongly with enhanced uptake in phagocytic J774 cells (R^2 = 0.99634), revealing an inverse relationship between protein corona abundance and internalization. However, the increased cellular uptake also heightened cytotoxicity in these cells.[178]

Conversely, a dense protein corona can shield GO from interacting with non-phagocytic cells such as A549, thereby suppressing uptake and mitigating cytotoxicity. In this case, reduced physical contact between the GO surface and the cell membrane minimizes adverse effects. Together, these observations support a ''protein corona by design'' strategy, wherein precise surface modifications enable control over corona composition and density, providing a tunable platform for decoding bio-nano interactions and advancing quality-by-design.

4.5 Controlling surface coating through 2D and layered material geometry

When examining the factors governing bio-interactions with 2D-material surfaces at the point of interaction, material identity at the end of interaction must be considered, which can be influenced by factors such as the functionalization medium (whether solvent-based or substrate-bound), as well as geometric properties like sheet size, surface area, edge shape (blunt, sharp or buckled), and thickness (which reflects the number of layers).

Thickness is often overlooked but plays a crucial role in determining the interaction strength. Also, factors related to crystallinity, such as structural defects and weak points, can significantly influence the final adsorption strength and the pattern of biomolecules on the surface.

When 2D materials are substrate-bound, their surface properties and electronic behavior can either mimic the underlying substrate or be altered slightly due to the transparency of the 2D material. This effect was demonstrated in a study that compared the interactions between amino acid-decorated tectomers with graphene and MoS_2. The study revealed that the number of layers and the substrate influence the overall adhesion strength. The adhesive pressure between customer-functionalized tips and monolayer (1L) graphene was nearly 25% higher than for monolayer (1L) MoS_2, highlighting chemical selectivity towards surface carbon and sulfur atoms.[161]

The interaction strength varied depending on the number of layers, with a clear order: 1L graphene > ML MoS_2 > 1L MoS_2 > 2L (folded) graphene > ML graphene. While adhesion to 1L graphene was initially stronger than to 1L MoS_2, the trend reversed with increasing layers, resulting in stronger adhesion to multilayer MoS_2 than multilayer graphene.[161]

The strength of these interactions is linked to the material's carrier type and the substrate effect. Graphene, typically a p-doped system on silica, exhibits a higher concentration of hole carriers in its monolayer, which decreases as layers increase, leading to stronger adhesion for 1L graphene. Since amino-terminated tectomers donate electrons, they bind more strongly to positively charged surfaces. In contrast, MoS_2, generally an n-doped system, experiences less n-doping with increasing layers due to charge screening and adsorbed impurities. This results in stronger adhesion for multilayer MoS_2, as tectomers donate more electrons to the increasingly positively charged MoS_2 layers.

4.6 Controlling (device) fabrication parameters at the atomic scale

Atomic-scale tuning of 2D and layered materials and devices is critical for achieving stable, long-term bio-interfaces. In aqueous environments, precise modification of patterned superlattices remains challenging—particularly when targeting asymmetric channels, tunable pore sizes, high crystallinity, and selective molecular transport, where van der Waals forces dominate interlayer interactions.[179] Layer-by-layer thinning techniques address some of these challenges by introducing controlled defects into MoS, WS_2 and bilayer WSe_2 heterostructures. Devices based on WSe_2/Si heterojunctions fabricated *via* such approaches exhibit ultrafast optoelectronic responses, underscoring their potential for bioelectronic applications.[179] Similarly, WS_2-based neural probes produced through atomic layer-by-layer etching achieve finely tuned monolayer thickness, restored surface quality, and high current on/off ratios, enhancing signal simulation fidelity.[180] Grain boundary engineering offers an additional route for atomic-level control, enabling improved charge mobility and doping efficiency in 2D sensors and memristors.[181] Quasi-bicrystal nanowelding, for example, creates atomically defined grain boundaries in bilayer h-BN, producing tailored molecular transport pathways (Fig. 11(a)).[182] Beyond sensing, neuromorphic computing also benefits from

such precision engineering. Organic–2D composites can emulate biological synaptic behavior, demonstrating stable bipolar resistive switching ($\sim 5 \times 10^2$ on/off ratio, >2400 cycles, 6000 s retention; Fig. 11(b)).[183] MXene-based ferroelectric synapses exhibit paired-pulse facilitation (~122% enhancement) and humidity-responsive photocurrent modulation (Fig. 11(c)).[181] Translating these material advances into bio-interfaces, dry and flexible MXene-based "MXtrodes" deliver high-fidelity neural recordings with low skin impedance (~2.8 kΩ at 1 kHz), comparable to Ag/AgCl electrodes, without requiring conductive gels.[139] Likewise, reduced graphene oxide (rGO) planar microelectrode arrays (MEAs) fabricated *via* laser reduction demonstrate long-term stability, high signal-to-noise ratios (8.5–12.0), and enhanced peak amplitudes (from 100 μV to 140 μV), with performance maintained over 100 hours *in vivo*. These rGO MEAs show superior electrocardiographic (ECG) recording capability compared with commercial counterparts, reinforcing the promise of atomic-scale engineering for next-generation bioelectronic platforms.[184]

Navigating biological barriers. As outlined in the previous sections, understanding and overcoming a hierarchy of biological barriers spanning systemic, tissue, cellular, and subcellular levels is crucial for 2D material translation. These barriers, including immune surveillance, membrane transport limitations, and tissue barrier penetration limitations, critically influence material biodistribution, stability, and functional performance. Barrier-specific strategies, from biomolecule-functionalized materials for blood–brain barrier crossing to tumor penetration, demonstrate the versatility of 2D materials for targeting specific tissues. Layered heterostructures and special coatings can also protect active interfaces from biodegradation *in vivo*. Understanding and engineering these multiscale interactions offers a rational framework for enabling reliable, high-performance biointerfaces that operate seamlessly within the complex physiological environments.

Degradation dynamics. The long-term performance of bio-integrated devices based on 2D materials is intrinsically linked to their stability in physiological environments. Recent *in vivo* and *in vitro* studies have mapped the degradation kinetics of 2D materials, revealing the central roles of immune cell interactions, enzymes, and the incorporation of degradation products into endogenous metabolic pathways.[37] For MoS_2, degradation in biofluids is highly sensitive to intrinsic structural defects, including grain boundaries, dislocations, and point defects. High-angle grain boundaries degrade more rapidly due to elevated defect densities and enhanced chemical reactivity, while point defects further accelerate dissolution. These findings underscore the defect-driven nature of degradation, suggesting that precise defect engineering can regulate device stability and functional lifespan.[185] In black phosphorus (BP), oxidative degradation initiates predominantly at the edges, producing phosphate-rich byproducts such as phosphates, phosphites, and other P_xO_y species.[186] These products can mimic endogenous ligands, potentially interfering with phosphorylation-dependent protein kinase signaling[187] and may pose systemic risks such as hyperphosphatemia.[188] Similar instability has been observed in BP-based constructs for

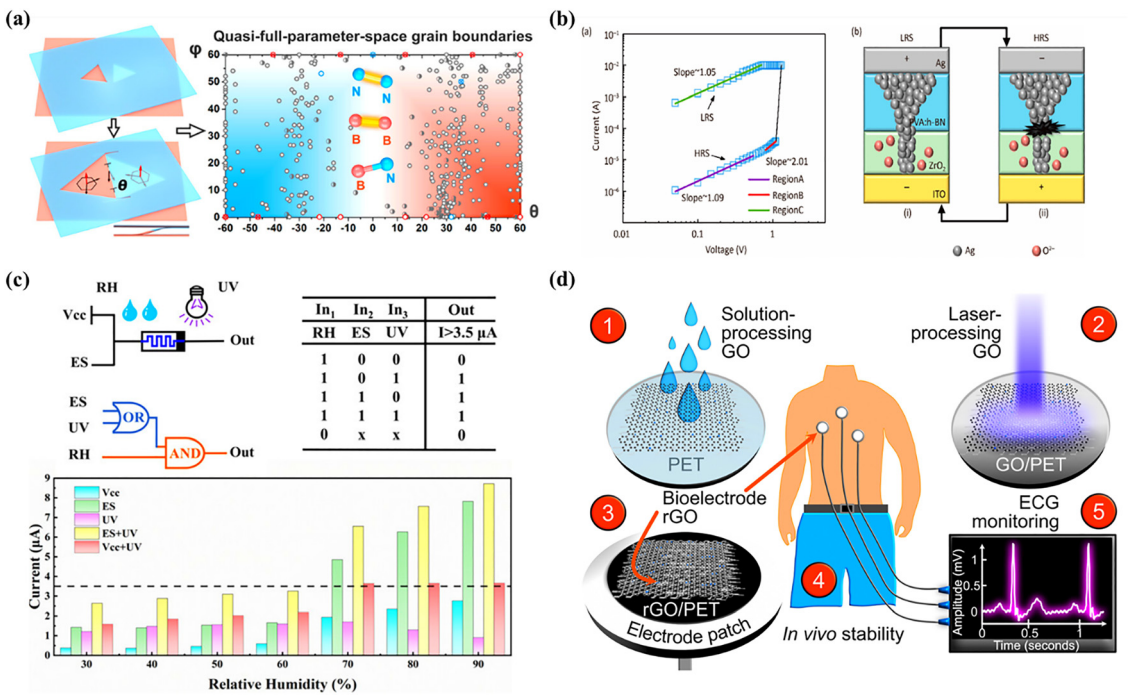

Fig. 11 (a) Schematic diagram of quasi-full-parameter-space grain boundaries (GBs) in 2D hexagonal boron nitride (h-BN)[182] (copyright 2019 *Letters*). (b) Schematic diagrams showing the high-resistance state (HRS) and low resistance state (LRS) of an organic–2D composite for the neuromorphic computing device[183] (copyright 2024 *J. Materiomics*). (c) Truth table logic gate circuit diagram and humidity response of the MXene/Y: HfO_2 memristor[181] (copyright 2024 *ACS Appl. Mater. Interfaces*). (d) Schematic showing processing steps for laser-reduced GO bioelectronics[184] (copyright 2020 https://pubs-acs-org.khalifa.idm.oclc.org/journal/aamick?ref=breadcrumb *Biosens. Bioelectron.*).

tissue regeneration, where rapid degradation compromises device performance.[189] MXenes, particularly $Ti_3C_2T_x$, combine high electrical conductivity with hydrophilicity and tunable surface terminations—features that also make them susceptible to moisture-induced degradation under physiological conditions.[190] Hybrid architectures incorporating MXenes with polymers or graphene have emerged as promising solutions, enhancing mechanical flexibility, chemical stability, and environmental resilience without sacrificing electrical performance.[190]

Protein adsorption dynamics. Protein adsorption is an early and decisive event governing the biological identity of 2D materials.[191] Adsorption behavior is dictated by surface energy, hydrogen bonding, steric effects, and electrostatic interactions, and is further modulated by the chemical composition and topology of the material surface. Proteins enriched in aromatic residues and disulfide bonds display high affinity for MoS_2 nanosheets, promoting the formation of stable coronas.[192] MXene nanosheets exhibit a pronounced preference for opsonins, leading to corona formation that increases particle size, reduces surface charge, and alters surface chemistry.[193] Such transformations influence downstream cellular interactions, with parameters including cell type, culture medium composition, and surface protein density collectively determining uptake, trafficking, and fate.[194]

Reactive oxygen species formation. The balance of reactive oxygen species (ROS) in biological systems is tightly regulated by antioxidant defenses, and disruption of this equilibrium is linked to inflammation, cytotoxicity, and carcinogenesis. Prolonged exposure to certain 2D materials can elevate ROS levels, impairing cell function and viability.

Graphene's long-term bio-performance is hindered by oxidative instability. GO, with carboxyl groups at its edges and epoxy/hydroxyl functionalities on its basal plane, offers enhanced biomolecular adsorption but is more susceptible to oxidative degradation. Conversely, amine-functionalized rGO exhibits greater chemical stability and biocompatibility, making it attractive for biomedical applications, though high production costs limit scalability.[195] ROS generation depends on multiple physicochemical parameters—size, shape, surface chemistry, dispersion stability, functionalization, and environmental pH[196]—and can lead to membrane disruption in immune cells such as macrophages, compromising viability.[197] The experimental context is also critical: *in vivo* and *in vitro* conditions can yield markedly different ROS profiles, influencing the interpretation of bio–nano interactions.

6. Conclusions, challenges and future prospects

Integrating 2D and layered materials into bioelectronic and optical platforms bridges nanoscale material functionality with complex biological systems. Their interactions with biological systems occur across multiple spatial and temporal scales and are influenced by parameters such as hydrophobicity, surface roughness, and reactive affinity. These factors determine protein corona composition, cellular adhesion, immune recognition, and systemic distribution, which together shape device performance and safety. Biodegradable and bioresorbable devices based on 2D materials are being explored for long-term integration with tissue. However, challenges remain, including biofouling, oxidative degradation, bacterial colonization, and material-specific instability. Hybrid designs that combine complementary materials and device engineering may help address these issues by improving stability and controlling reactivity. Further progress depends on *in vivo* studies under realistic physiological conditions and on surface engineering strategies that stabilize materials and modulate protein adsorption. Improvements in atomic-scale fabrication and microstructuring could enable devices with controlled transport properties and higher sensing precision.

Approaches such as ''nanoimmunity-by-design,'' combined with computational modelling and scalable manufacturing, may support the development of devices with predictable biological responses. Ultimately, translating 2D and layered materials into clinically viable biointegrated devices will require a holistic approach that integrates atomic-scale engineering, dynamic biointerface modulation, and systemic biological compatibility. Advances in biomimetic surface functionalization, hybrid material design, nanoimmunity-informed engineering, and artificial intelligence-driven predictive tools could help overcome barriers such as biofouling, immune clearance, reproducibility, and scalability. Achieving a detailed understanding and precise control of biointerfaces will be key to producing devices capable of long-term, seamless integration with human physiology.

Continued integration of materials science, biointerface engineering, and biological evaluation will be important for creating reliable devices for applications in diagnostics, therapeutics, and monitoring.

Conflicts of interest

There are no conflicts to declare.

Data availability

There are no data availabile as this is a review article.

Acknowledgements

AMP and NY acknowledge funding from the NIH-Al Jalila collaborative grant (AJF-NIH-19-KU). AMP and NM acknowledge the Biotechnology Center, Khalifa University. AMP, NM, YS and LD acknowledge funding from the Research & Innovation Center for Graphene and 2D materials (RIC-2D), Khalifa University. AMP acknowledges funding from the Center for Catalysis and Separation (CeCaS), Khalifa University, UAE. AMP and LD also acknowledge the funding support from the European Union's Horizon Europe program under the Marie Sklodowska-Curie grant agreement no. 101086184 (MX-MAP). For this

review, we used large language models, including ChatGPT (OpenAI) and Claude (Anthropic), to correct the grammar and wording of the text. All text in the manuscript was written by the authors, and large language models were used solely for style corrections with no input in the content or meaning.

References

1 M. Jaber and J. Miehé-Brendlé, *Ordered porous solids*, Elsevier, 2009, pp. 31–49.
2 E. Davies, *J. Inclusion Phenom.*, 1983, **1**, 209.
3 P. Avouris, T. F. Heinz and T. Low, *2D Materials*, Cambridge University Press, 2017.
4 T. Schmaltz, L. Wormer, U. Schmoch and H. Döscher, *2D Mater.*, 2024, **11**, 022002.
5 S. Yadav, B. Kumar and S. Kaushik, *Appl. Surf. Sci. Adv.*, 2023, **18**, 100512.
6 J. Miao and T. Fan, *Carbon*, 2023, **202**, 495–527.
7 L. Cao, C. Wang and Y. Huang, *Chem. Eng. J.*, 2023, **454**, 140094.
8 P. S. Reddy, *Micromater. Interfaces*, 2024, **2**, 6377.
9 A. Nag, A. Mitra and S. C. Mukhopadhyay, *Sens. Actuators, A*, 2018, **270**, 177–194.
10 T.-H. Han, H. Kim, S.-J. Kwon and T.-W. Lee, *Mater. Sci. Eng., R*, 2017, **118**, 1–43.
11 A. A. AbdelHamid, A. Elgamouz and A.-N. Kawde, *RSC Adv.*, 2023, **13**, 21300–21312.
12 G. Cai, Z. Liu, J. Yang, H. Xie, X. Yu and B. Zheng, *J. Mater. Chem. C*, 2024, **12**, 15339–15358.
13 H. Chen, L. Li, T. Zhang, Z. Qiao, J. Tang and J. Zhou, *J. Phys. Chem. C*, 2018, **122**, 2070–2080.
14 A. Esteghamat and O. Akhavan, *Microelectron. Eng.*, 2023, **267**, 111899.
15 Z. Huang, B. Liu and J. Liu, *Langmuir*, 2019, **35**, 9858–9866.
16 A. Kumar, L. Viscardi, E. Faella, F. Giubileo, K. Intonti, A. Pelella, S. Sleziona, O. Kharsah, M. Schleberger and A. Di Bartolomeo, *J. Mater. Sci.*, 2023, **58**, 2689–2699.
17 R. Qiao, C. Fu, H. Forgham, I. Javed, X. Huang, J. Zhu, A. K. Whittaker and T. P. Davis, *Adv. Drug Delivery Rev.*, 2023, **197**, 114822.
18 S. Tamilvanan and A. Ramadoss, *Hexagonal Boron Nitride*, Elsevier, 2024, pp. 295–319.
19 R. Zribi, G. Neri and E. Proverbio, 2023.
20 G. Gorle, G. Gollavelli, G. Nelli and Y.-C. Ling, *Pharmaceutics*, 2023, **15**, 632.
21 S. Natarajan, J. Joseph and D. M. F. Prazeres, *Sens. Actuators, B*, 2023, **393**, 134336.
22 E. Cojocaru, M. Oprea, G. M. Vlăsceanu, M.-C. Nicolae, R.-C. Popescu, P.-E. Mereuță, A.-G. Toader and M. Ioniță, *RSC Adv.*, 2024, **14**, 32517–32532.
23 K. Asif, M. M. Rahman, A. A. Sfriso, S. Parisi, V. Canzonieri, I. Caligiuri, F. Rizzolio and M. Adeel, *RSC Adv.*, 2024, **14**, 26568–26579.
24 N. Dogra, P. Agrawal, S. Pathak, R. Saini and S. Sharma, *Int. J. Hydrogen Energy*, 2023, **48**, 26210–26220.
25 C. Liu, S. Ding, Q. Tian, X. Hong, W. Su, L. Tang, L. Wang, M. Zhang, X. Liu and Y. Lv, *Laser Photonics Rev.*, 2023, **17**, 2200486.
26 S. Jiang, J. Lin and P. Huang, *Adv. Healthcare Mater.*, 2023, **12**, 2202208.
27 W. Yao, T. Yang, D. Liu, F. Liu, L. Zhang, C. Cheng, J. Hu and H. Huang, *J. Alloys Compd.*, 2024, **1004**, 175848.
28 X. Zhu, A. Huang, I. Martens, N. Vostrov, Y. Sun, M. I. Richard, T. U. Schülli and L. Wang, *Adv. Mater.*, 2024, 2403482.
29 M. Ni, Q. Xia, J. Liu, X. Zhu and H. Xia, *Energy Fuels*, 2024, **38**, 12228–12238.
30 L. Fusco, A. Gazzi, C. E. Shuck, M. Orecchioni, D. Alberti, S. M. D'Almeida, D. Rinchai, E. Ahmed, O. Elhanani and M. Rauner, *Adv. Mater.*, 2022, **34**, 2205154.
31 G. Cooksley, M. K. Dymond, N. A. Stewart, G. Bucca, A. Hesketh, J. Lacey, Y. Gogotsi and S. Sandeman, *2D Mater.*, 2022, **10**, 014003.
32 H. Zhang, S. Sun, X. Shang, B. Guo, X. Li, X. Chen, S. Jiang, H. Zhang, H. Ågren, W. Zhang, G. Wang, C. Lu and S. Fu, *Nanophotonics*, 2022, **11**, 1261–1284.
33 B. You, J. Yoon, Y. Kim, M. Yang, J. Bak, J. Park, U. J. Kim, M. G. Hahm and M. Lee, *J. Mater. Chem. C*, 2024, **12**, 6596–6605.
34 T. Zahra, U. Javeria, H. Jamal, M. M. Baig, F. Akhtar and U. Kamran, *Anal. Chim. Acta*, 2024, **1316**, 342880.
35 K. Kostarelos and K. S. Novoselov, *Nat. Nanotechnol.*, 2014, **9**, 744–745.
36 M. Cao, R. Cai, L. Zhao, M. Guo, L. Wang, Y. Wang, L. Zhang, X. Wang, H. Yao and C. Xie, *Nat. Nanotechnol.*, 2021, **16**, 708–716.
37 S. Vranic, R. Kurapati, K. Kostarelos and A. Bianco, *Nat. Rev. Chem.*, 2025, **9**, 173–184.
38 A. Yadav, H. Kumar, R. Sharma and R. Kumari, *Surf. Interfaces*, 2023, **39**, 102925.
39 S. Rabbani, Z. Qureshi, A. Alfantazi, A. Alkaabi, S. Alameri, Y. Addad, Y. Samad and I. Afgan, *2D Mater.*, 2024, **11**, 042001.
40 Z.-K. Liu, J.-L. Ling, Y.-Y. Liu, B.-H. Zheng and C.-D. Wu, *Chem. Commun.*, 2024, **60**, 12964–12976.
41 K. A. Su, S. Li, W.-C. Wen, Y. Yamamoto and M. S. Arnold, *RSC Adv.*, 2024, **14**, 25378–25384.
42 A. Sutorius, R. Weißing, C. R. Pèrez, T. Fischer, F. Hartl, N. Basu, H. S. Shin and S. Mathur, *Nanoscale*, 2024, **16**, 15782–15792.
43 R. Kumar, N. Goel, D. K. Jarwal, Y. Hu, J. Zhang and M. Kumar, *J. Mater. Chem. C*, 2023, **11**, 774–801.
44 T. Kang, T. W. Tang, B. Pan, H. Liu, K. Zhang and Z. Luo, *ACS Mater. Au*, 2022, **2**, 665–685.
45 V. Thirumal, R. Yuvakkumar, P. S. Kumar, G. Ravi, S. Keerthana and D. Velauthapillai, *Chemosphere*, 2022, **286**, 131733.
46 M. Tripathi, G. Deokar, J. Casanova-Chafer, J. Jin, A. Sierra-Castillo, S. Ogilvie, F. Lee, S. A. Iyengar, A. Biswas and E. Haye, *Nanoscale Horiz.*, 2024, **9**, 1330–1340.
47 J. Wang, G. Yang, Y. Jiao, H. Yan and H. Fu, *Small Methods*, 2025, **9**, 2301602.

48 E. S. Polsen, D. Q. McNerny, B. Viswanath, S. W. Pattinson and A. John Hart, *Sci. Rep.*, 2015, **5**, 1–12.
49 M. Cao, S. Li, L. Nie and Y. Chen, *Mater. Today Sustain.*, 2023, **24**, 100522.
50 S. Sigdel, J. P. Wright, J. Covarrubias, A. Sekar, K. Mutthukumar, S. H. Bossmann, J. Li, A. Nepal, S. Corkill and C. M. Sorensen, *Carbon Trends*, 2023, **13**, 100306.
51 M. Xu, J. Gao, J. Song, H. Wang, L. Zheng, Y. Wei, Y. He, X. Wang and W. Huang, *iScience*, 2021, **24**, 103313.
52 R. You, Y. Q. Liu, Y. L. Hao, D. D. Han, Y. L. Zhang and Z. You, *Adv. Mater.*, 2020, **32**, 1901981.
53 Y. Lv, L. Yu, C. Jiang, S. Chen and Z. Nie, *RSC Adv.*, 2014, **4**, 13350–13354.
54 H. Yu, B. Zhang, C. Bulin, R. Li and R. Xing, *Sci. Rep.*, 2016, **6**, 36143.
55 E. B. Secor, S. Lim, H. Zhang, C. D. Frisbie, L. F. Francis and M. C. Hersam, *Adv. Mater.*, 2014, **26**, 4533–4538.
56 K. R. Paton, E. Varrla, C. Backes, R. J. Smith, U. Khan, A. O'Neill, C. Boland, M. Lotya, O. M. Istrate and P. King, *Nat. Mater.*, 2014, **13**, 624–630.
57 P. G. Karagiannidis, S. A. Hodge, L. Lombardi, F. Tomarchio, N. Decorde, S. Milana, I. Goykhman, Y. Su, S. V. Mesite and D. N. Johnstone, *ACS Nano*, 2017, **11**, 2742–2755.
58 J. Chen, M. Xiao, Z. Chen, S. Khan, S. Ghosh, N. Macadam, Z. Chen, B. Zhou, G. Yun and K. Wilk, *arXiv*, 2023, preprint, arXiv:2312.16501, DOI: **10.48550/arXiv:2312.16501**.
59 H. V. Padi, N. Nanattil, S. Sulaiman, R. M. Ramakrishnan and B. N. Narayanan, *J. Energy Storage*, 2024, **86**, 111297.
60 J.-M. Jeong, H. Kang, H.-J. Kim, S. B. Hong, H. Jeon, S. Hwang, D. Seo, B. Kwak, Y.-K. Han, B. Choi and D. Kim, *Adv. Funct. Mater.*, 2018, **28**, 1802952.
61 K. Parvez, R. Li, S. R. Puniredd, Y. Hernandez, F. Hinkel, S. Wang, X. Feng and K. Müllen, *ACS Nano*, 2013, **7**, 3598–3606.
62 X. Fan, X. Zhang, Y. Li, H. He, Q. Wang, L. Lan, W. Song, T. Qiu and W. Lu, *Nanoscale Horiz.*, 2023, **8**, 309–319.
63 S. S. Nemala, J. Fernandes, J. Rodrigues, V. Lopes, R. M. Pinto, K. Vinayakumar, E. Placidi, G. De Bellis, P. Alpuim and R. S. Sampaio, *Nano Energy*, 2024, **127**, 109781.
64 A. D. R. Castillo, V. Pellegrini, A. Ansaldo, F. Ricciardella, H. Sun, L. Marasco, J. Buha, Z. Dang, L. Gagliani and E. Lago, *Mater. Horiz.*, 2018, **5**, 890–904.
65 M. A. Molina-Garcia, S. Bellani, A. E. D. R. Castillo, I. Conticello, L. Gabatel, M. I. Zappia, M. Eredia, S. Thorat, B. Martin-Garcia and L. Ceseracciu, *J. Phys.: Mater.*, 2023, **6**, 035006.
66 S. Bellani, E. Petroni, A. E. Del Rio Castillo, N. Curreli, B. Martín-García, R. Oropesa-Nuñez, M. Prato and F. Bonaccorso, *Adv. Funct. Mater.*, 2019, **29**, 1807659.
67 Y. Bu, R. B. Cabulong and B. S. Kim, *Green Chem.*, 2024, **26**, 3488–3506.
68 L. Zhou, B. Zhang, F. Li, Y. Yan, Y. Wang and R. Li, *Nanoscale Adv.*, 2023, **5**, 6582–6593.
69 L. Zhou, K. Wang, H. Sun, S. Zhao, X. Chen, D. Qian, H. Mao and J. Zhao, *Nano-Micro Lett.*, 2019, **11**, 1–13.
70 R. Jin, N. Brljak, J. M. Slocik, R. Rao, M. R. Knecht and T. R. Walsh, *J. Mater. Chem. B*, 2024, **12**, 4824–4832.
71 M. Ayan-Varela, O. Perez-Vidal, J. I. Paredes, J. M. Munuera, S. Villar-Rodil, M. Díaz-González, C. Fernandez-Sanchez, V. S. Silva, M. Cicuéndez and M. Vila, *ACS Appl. Mater. Interfaces*, 2017, **9**, 2835–2845.
72 A. Pattammattel, P. Pande, D. Kuttappan, M. Puglia, A. K. Basu, M. A. Amalaradjou and C. V. Kumar, *Langmuir*, 2017, **33**, 14184–14194.
73 V.-T. Nguyen, P. A. Le, Y.-C. Hsu and K.-H. Wei, *ACS Appl. Mater. Interfaces*, 2020, **12**, 11533–11542.
74 Y. Liu, Q. Tang, M. Xu, J. Ren, C. Guo, C. Chen, W. Geng, W. Lei, X. Zhao and D. Liu, *Chem. Eng. J.*, 2023, **468**, 143439.
75 G. Seo, G. Lee, M. J. Kim, S.-H. Baek, M. Choi, K. B. Ku, C.-S. Lee, S. Jun, D. Park and H. G. Kim, *ACS Nano*, 2020, **14**, 5135–5142.
76 G. Dastgeer, Z. M. Shahzad, H. Chae, Y. H. Kim, B. M. Ko and J. Eom, *Adv. Funct. Mater.*, 2022, **32**, 2204781.
77 J. An, H. Park, J. Kim, H. Park, T.-H. Kim, C. Park, J. Kim, M.-H. Lee and T. Lee, *ACS Sens.*, 2023, **8**, 3174–3186.
78 X. Chen, Q. Li, T. Yuan, M. Ma, Z. Ye, X. Wei, X. Fang and S. Mao, *ACS Sens.*, 2023, **8**, 858–866.
79 R. Zhou, B. Tu, D. Xia, H. He, Z. Cai, N. Gao, G. Chang and Y. He, *Anal. Chim. Acta*, 2022, **1201**, 339653.
80 J. L. Gogola, G. Martins, A. Gevaerd, L. Blanes, J. Cardoso, F. K. Marchini, C. E. Banks, M. F. Bergamini and L. H. Marcolino-Junior, *Anal. Chim. Acta*, 2021, **1166**, 338548.
81 N. Özcan, H. Medetalibeyoglu, O. Akyıldırım, N. Atar and M. L. Yola, *Mater. Today Commun.*, 2020, **23**, 101097.
82 Z. Yang, H. Guo, Z. Yu, M. Wang, X. Wei, Z. Lu, L. Sun, H. Ren and W. Yang, *Chem. Eng. J.*, 2024, **492**, 152271.
83 W. Ling, Y. Hao, H. Wang, H. Xu and X. Huang, *Nanotechnology*, 2019, **30**, 424002.
84 Y. Zhang, C. Li, A. Guo, Y. Yang, Y. Nie, J. Liao, B. Liu, Y. Zhou, L. Li and Z. Chen, *Nat. Commun.*, 2024, **15**, 1618.
85 S. Xiong, S. Ye, P. Ni, M. Zhong, J. Shan, T. Yuan, J. Liang, Y. Fan and X. Zhang, *Carbohydr. Polym.*, 2023, **319**, 121172.
86 Y. Lu, G. Yang, S. Wang, Y. Zhang, Y. Jian, L. He, T. Yu, H. Luo, D. Kong and Y. Xianyu, *Nat. Electron.*, 2024, **7**, 51–65.
87 C. Xu, X. Chen, Q. Wang, L. Zhang, X. Gao, X. Yang, L. Yang, X. Liu, X. Wang and Y. Wang, *Adv. Funct. Mater.*, 2024, **34**, 2310168.
88 Y. Xiang, J. Liu, J. Chen, M. Xiao, H. Pei and L. Li, *ACS Appl. Mater. Interfaces*, 2024, **16**, 15861–15869.
89 F. Zhang, G. Sun, R. Zhao, F. Yang, X. Jiang, S. Song, J. Zhang, H. Shen and J. Shen, *Langmuir*, 2024, **40**, 11381–11389.
90 J. Zeng, C. Gu, X. Geng, K. Lin, Y. Xie and X. Chen, *Biomaterials*, 2023, **297**, 122122.
91 K. Balamurugan, E. A. Singam and V. Subramanian, *J. Phys. Chem. C*, 2011, **115**, 8886–8892.
92 Z. Gu, Z. Yang, Y. Chong, C. Ge, J. K. Weber, D. R. Bell and R. Zhou, *Sci. Rep.*, 2015, **5**, 10886.
93 K. C. Mei, A. Ghazaryan, E. Z. Teoh, H. D. Summers, Y. Li, B. Ballesteros, J. Piasecka, A. Walters, R. C. Hider and V. Mailänder, *Adv. Mater.*, 2018, **30**, 1802732.

94 M. Han, O. Karatum and S. Nizamoglu, *ACS Appl. Mater. Interfaces*, 2022, **14**, 20468–20490.
95 R. Janissen, P. K. Sahoo, C. A. Santos, A. M. Da Silva, A. A. Von Zuben, D. E. Souto, A. D. Costa, P. Celedon, N. I. Zanchin and D. B. Almeida, *Nano Lett.*, 2017, **17**, 5938–5949.
96 P. K. Sahoo, R. Janissen, M. P. Monteiro, A. Cavalli, D. M. Murillo, M. V. Merfa, C. L. Cesar, H. F. Carvalho, A. A. De Souza and E. P. Bakkers, *Nano Lett.*, 2016, **16**, 4656–4664.
97 T. Tene, Y. Jiménez-Gaona, D. K. Campoverde-Santos, Y. Cevallos, M. La Pietra, C. Vacacela Gomez, A. Scarcello, S. Straface, L. S. Caputi and S. Bellucci, *Front. Chem.*, 2023, **11**, 1267199.
98 C. Choi, Y. Lee, K. W. Cho, J. H. Koo and D.-H. Kim, *Acc. Chem. Res.*, 2018, **52**, 73–81.
99 H.-L. Peng, Y.-l Sun, C. Bi and Q.-F. Li, *Measurement*, 2022, **190**, 110782.
100 N. Driscoll, B. Erickson, B. B. Murphy, A. G. Richardson, G. Robbins, N. V. Apollo, G. Mentzelopoulos, T. Mathis, K. Hantanasirisakul and P. Bagga, *Sci. Transl. Med.*, 2021, **13**, eabf8629.
101 A. S. Sharbirin, S. Roy, T. T. Tran, S. Akhtar, J. Singh, D. L. Duong and J. Kim, *J. Mater. Chem. C*, 2022, **10**, 6508–6514.
102 K. Dolui and S. Y. Quek, *Sci. Rep.*, 2015, **5**, 11699.
103 H.-Y. Ren, Y. Mao, Y.-N. Ren, Q.-F. Sun and L. He, *ACS Nano*, 2024, **19**, 1352–1360.
104 J. Gong, H. Tang, M. Wang, X. Lin, K. Wang and J. Liu, *Mater. Des.*, 2022, **215**, 110506.
105 J. Linares, M. C. n Matesanz, M. Vila, M. J. Feito, G. Goncalves, M. Vallet-Regi, P. A. Marques and M. T. Portolés, *ACS Appl. Mater. Interfaces*, 2014, **6**, 13697–13706.
106 B. Fatma, S. M. Andrabi, S. Gupta, V. Verma, A. Kumar, C. Pitsalidis and A. Garg, *Nano Energy*, 2023, **114**, 108628.
107 N. Driscoll, A. G. Richardson, K. Maleski, B. Anasori, O. Adewole, P. Lelyukh, L. Escobedo, D. K. Cullen, T. H. Lucas and Y. Gogotsi, *ACS Nano*, 2018, **12**, 10419–10429.
108 S. Yin, Y. L. Wu, B. Hu, Y. Wang, P. Cai, C. K. Tan, D. Qi, L. Zheng, W. R. Leow and N. S. Tan, *Adv. Mater. Interfaces*, 2014, **1**, 1300043.
109 X. Wang, A. Liu, Y. Xing, H. Duan, W. Xu, Q. Zhou, H. Wu, C. Chen and B. Chen, *Biosens. Bioelectron.*, 2018, **105**, 22–28.
110 S. Patra, E. Roy, A. Tiwari, R. Madhuri and P. K. Sharma, *Biosens. Bioelectron.*, 2017, **89**, 8–27.
111 S. Kumar, S. M. Z. Mehdi and Y. Seo, *Small*, 2024, **20**, 2405576.
112 M. Byakodi, N. S. Shrikrishna, R. Sharma, S. Bhansali, Y. Mishra, A. Kaushik and S. Gandhi, *Biosens. Bioelectron.: X*, 2022, **12**, 100284.
113 T. Li, W. Qiang and B. Lei, *Nanoscale*, 2025, **17**, 4854–4891.
114 M. Loeblein, G. Perry, S. H. Tsang, W. Xiao, D. Collard, P. Coquet, Y. Sakai and E. H. T. Teo, *Adv. Healthcare Mater.*, 2016, **5**, 1177–1191.
115 T. R. Dmytriv and V. I. Lushchak, *Chem. Rec.*, 2024, **24**, e202300338.
116 F. Ruan, R. Liu, K. Wang, J. Zeng, Z. Zuo, C. He and Y. Zhang, *J. Hazard. Mater.*, 2021, **402**, 122875.
117 K. Arab, A. Jafari and F. Shahi, *Polym. Adv. Technol.*, 2024, **35**, e6571.
118 O. Anwar, A. S. Amin, A. Amin, M. A. Kräenbring, F. Özcan and D. Segets, *Part. Part. Syst. Charact.*, 2023, **40**, 2300050.
119 A. S. Sarkar and E. Stratakis, *J. Colloid Interface Sci.*, 2021, **594**, 334–341.
120 C. M. Hansen, *Hansen solubility parameters: a user's handbook*, CRC press, 2007.
121 D. Nakamura, M. Hirano and R. Ohta, *Chem. Commun.*, 2017, **53**, 4096–4099.
122 A. O'Neill, U. Khan, P. N. Nirmalraj, J. Boland and J. N. Coleman, *J. Phys. Chem. C*, 2011, **115**, 5422–5428.
123 J. Occhiuzzi, G. G. Politano, G. D'Olimpio and A. Politano, *Molecules*, 2023, **28**, 1484.
124 Z. Zhou, L. Li, X. Liu, H. Lei, W. Wang, Y. Yang, J. Wang and Y. Cao, *J. Mol. Liq.*, 2021, **324**, 115116.
125 J. Ma, X. Nan, J. Liu, W. Zhu and W. Qin, *Mater. Today Commun.*, 2018, **14**, 99–105.
126 C. T. Castillo, C. Bruel and J. R. Tavares, *Nanoscale Adv.*, 2020, **2**, 2497–2506.
127 S. Claridge, *Chem. Commun.*, 2018, **54**, 6681–6691.
128 Y. Tu, M. Lv, P. Xiu, T. Huynh, M. Zhang, M. Castelli, Z. Liu, Q. Huang, C. Fan and H. Fang, *Nat. Nanotechnol.*, 2013, **8**, 594–601.
129 Z. Chen, X. Lu, J. Liu, X. Tian, W. Li, K. Yang and B. Yuan, *J. Phys. Chem. B*, 2021, **125**, 3589–3597.
130 D. Wu, R. Zhao, Y. Chen, Y. Wang, J. Li and Y. Fan, *Phys. Chem. Chem. Phys.*, 2021, **23**, 3341–3350.
131 C. L. Manzanares-Palenzuela, A. M. Pourrahimi, J. Gonzalez-Julian, Z. Sofer, M. Pykal, M. Otyepka and M. Pumera, *Chem. Sci.*, 2019, **10**, 10010–10017.
132 T. R. Walsh and M. R. Knecht, *Bioconjugate Chem.*, 2019, **30**, 2727–2750.
133 S. Roy, Aastha, K. A. Deo, K. Dey, A. K. Gaharwar and A. Jaiswal, *ACS Appl. Mater. Interfaces*, 2023, **15**, 35753–35787.
134 H. Zhang, T. Yamazaki, C. Zhi and N. Hanagata, *Nanoscale*, 2012, **4**, 6343–6350.
135 C. Valentina, Z. Weitao, B. Luca, L. G. M. Cristina, F. G. Meder, P. Ester, R. Paton Keith, B. Claudia, N. Coleman Jonathan and A. Dawson Kenneth, *Nat. Commun.*, 2018, **9**, 1577.
136 J. H. Shannahan, X. Lai, P. C. Ke, R. Podila, J. M. Brown and F. A. Witzmann, *PLoS One*, 2013, **8**, e74001.
137 V. Castagnola, W. Zhao, L. Boselli, M. C. Lo Giudice, F. Meder, E. Polo, K. Paton, C. Backes, J. Coleman and K. Dawson, *Nat. Commun.*, 2018, **9**, 1577.
138 C. Braccia, V. Castagnola, E. Vázquez, V. J. González, F. Loiacono, F. Benfenati and A. Armirotti, *Carbon*, 2021, **185**, 591–598.
139 M. Mahmoudi, M. P. Landry, A. Moore and R. Coreas, *Nat. Rev. Mater.*, 2023, **8**, 422–438.

140 J. S. Rowlinson and B. Widom, *Molecular theory of capillarity*, Courier Corporation, 2013.
141 K. A. Dawson and Y. Yan, *Nat. Nanotechnol.*, 2021, **16**, 229–242.
142 S. Milani, F. Baldelli Bombelli, A. S. Pitek, K. A. Dawson and J. Radler, *ACS Nano*, 2012, **6**, 2532–2541.
143 M. Kokkinopoulou, J. Simon, K. Landfester, V. Mailänder and I. Lieberwirth, *Nanoscale*, 2017, **9**, 8858–8870.
144 A. Baszkin and W. Norde, *Physical chemistry of biological interfaces*, CRC Press, 1999.
145 T. Seki, C. R. So, T. R. Page, D. Starkebaum, Y. Hayamizu and M. Sarikaya, *Langmuir*, 2018, **34**, 1819–1826.
146 M. A. Unal, F. Bayrakdar, H. Nazir, O. Besbinar, C. Gurcan, N. Lozano, L. M. Arellano, S. Yalcin, O. Panatli and D. Celik, *Small*, 2021, **17**, 2101483.
147 D. Gao, B. Li, Y. Yang, Y. Qu, Y.-Q. Li, M. Zhao, Y. Liu, X. Liu and W. Li, *J. Phys. Chem. B*, 2021, **125**, 2833–2840.
148 S. N. Kim, Z. Kuang, J. M. Slocik, S. E. Jones, Y. Cui, B. L. Farmer, M. C. McAlpine and R. R. Naik, *J. Am. Chem. Soc.*, 2011, **133**, 14480–14483.
149 L. Rodríguez-Pérez, M. Á. Herranz and N. Martín, *Chem. Commun.*, 2013, **49**, 3721–3735.
150 C. Gautam and S. Chelliah, *RSC Adv.*, 2021, **11**, 31284–31327.
151 J. Kaur, A. Vergara, M. Rossi, A. M. Gravagnuolo, M. Valadan, F. Corrado, M. Conte, F. Gesuele, P. Giardina and C. Altucci, *RSC Adv.*, 2017, **7**, 50166–50175.
152 M. Golda-Cepa, D. Kumar, M. Bialoruski, S. Lasota, Z. Madeja, W. Piskorz and A. Kotarba, *J. Mater. Chem. B*, 2023, **11**, 4946–4957.
153 X. Liu and M. C. Hersam, *Adv. Mater.*, 2018, **30**, 1801586.
154 L. Rodrıguez-Pérez, M. Á. Herranz and N. Martın, *Chem. Commun.*, 2013, **49**, 3721–3735.
155 S. Ippolito, A. Ciesielski and P. Samorì, *Chem. Commun.*, 2019, **55**, 8900–8914.
156 J. D. Schneible, K. Shi, A. T. Young, S. Ramesh, N. He, C. E. Dowdey, J. M. Dubnansky, R. L. Lilova, W. Gao and E. Santiso, *J. Mater. Chem. B*, 2020, **8**, 3852–3868.
157 K. H. Ibrahim, M. Irannejad, B. Wales, J. Sanderson, M. Yavuz and K. P. Musselman, *Adv. Opt. Mater.*, 2018, **6**, 1701365.
158 S. Huang, R. Pandey, I. Barman, J. Kong and M. Dresselhaus, *ACS Photonics*, 2018, **5**, 2978–2982.
159 R. Kurapati, F. Bonachera, J. Russier, A. R. Sureshbabu, C. Ménard-Moyon, K. Kostarelos and A. Bianco, *2D Mater.*, 2017, **5**, 015020.
160 G. Unnikrishnan, A. Joy, M. Megha, J. Thomas, M. Haris, E. Kolanthai and S. Muthuswamy, *New J. Chem.*, 2024, **48**, 8908–8925.
161 M. Tripathi, R. Garriga, F. Lee, S. P. Ogilvie, A. A. Graf, M. J. Large, P. J. Lynch, K. Papagelis, J. Parthenios and V. L. Cebolla, *2D Mater.*, 2022, **9**, 045033.
162 R. Garriga, I. Jurewicz, S. Seyedin, N. Bardi, S. Totti, B. Matta-Domjan, E. G. Velliou, M. A. Alkhorayef, V. L. Cebolla and J. M. Razal, *Nanoscale*, 2017, **9**, 7791–7804.
163 A. Gazzi, L. Fusco, M. Orecchioni, S. Ferrari, G. Franzoni, J. S. Yan, M. Rieckher, G. Peng, M. A. Lucherelli and I. A. Vacchi, *J. Phys.: Mater*, 2020, **3**, 034009.
164 M. Orecchioni, D. Bedognetti, L. Newman, C. Fuoco, F. Spada, W. Hendrickx, F. M. Marincola, F. Sgarrella, A. F. Rodrigues and C. Ménard-Moyon, *Nat. Commun.*, 2017, **8**, 1109.
165 P. Nicolussi, G. Pilo, M. G. Cancedda, G. Peng, N. D. Q. Chau, A. De la Cadena, R. Vanna, Y. A. Samad, T. Ahmed and J. Marcellino, *Adv. Healthcare Mater.*, 2024, 2401783.
166 C. Rive, G. Reina, P. Wagle, E. Treossi, V. Palermo, A. Bianco, L. G. Delogu, M. Rieckher and B. Schumacher, *Small*, 2019, **15**, 1902699.
167 J. Russier, V. León, M. Orecchioni, E. Hirata, P. Virdis, C. Fozza, F. Sgarrella, G. Cuniberti, M. Prato and E. Vázquez, *Angew. Chem., Int. Ed.*, 2017, **56**, 3014–3019.
168 L. Fusco, E. Avitabile, V. Armuzza, M. Orecchioni, A. Istif, D. Bedognetti, T. Da Ros and L. G. Delogu, *Carbon*, 2020, **160**, 390–404.
169 M. D. McCauley, F. Vitale, J. S. Yan, C. C. Young, B. Greet, M. Orecchioni, S. Perike, A. Elgalad, J. A. Coco and M. John, *Circ.: Arrhythmia Electrophysiol.*, 2019, **12**, e007256.
170 W. Dong, S. Zhao, Y. Wang, X. Zhou, J. Jiang, J. Dang, D. Sun, X. Dai, M. Zhang and Z. Jiang, *Mater. Des.*, 2023, **225**, 111485.
171 Y. Wang, J. E. Hartung, A. Goad, M. A. Preisegger, B. Chacon, M. S. Gold, Y. Gogotsi and T. Cohen-Karni, *Adv. Healthcare Mater.*, 2024, **13**, 2302330.
172 R. Zizhou, S. Baratchi, K. Khoshmanesh, X. Wang and S. Houshyar, *ACS Appl. Nano Mater.*, 2024, **7**, 9757–9767.
173 S. Roy, P. Haloi, S. Chawla, V. B. Konkimalla and A. Jaiswal, *J. Mater. Chem. B*, 2023, **11**, 10418–10432.
174 J. H. Lee, S. M. Baek, G. Lee, S.-J. Kim, H. S. Kim and S. K. Hahn, *ACS Appl. Bio Mater.*, 2020, **3**, 8879–8889.
175 Z. Yuan, B. Tao, Y. He, J. Liu, C. Lin, X. Shen, Y. Ding, Y. Yu, C. Mu and P. Liu, *Biomaterials*, 2019, **217**, 119290.
176 P. Fathi-Hafshejani, H. B. Tinker, K. Freel, M. Mahjouri-Samani and S. Hasim, *ACS Appl. Bio Mater.*, 2023, **6**, 436–444.
177 A. Gazzi, L. Fusco, M. Orecchioni, S. Keshavan, Y. Shin, J.-C. Grivel, D. Rinchai, E. I. Ahmed, O. Elhanani and G. Furesi, *Nano Today*, 2024, **54**, 102084.
178 L. Baweja, K. Balamurugan, V. Subramanian and A. Dhawan, *Langmuir*, 2013, **29**, 14230–14238.
179 P. M. Das, J. P. Thiruraman, M.-Q. Zhao, S. V. Mandyam, A. C. Johnson and M. Drndić, *Nanotechnology*, 2019, **31**, 105302.
180 Y. You, J. Park and J. Kim, *ECS J. Solid State Sci. Technol.*, 2023, **12**, 075009.
181 J. Fang, Z. Tang, X.-C. Lai, F. Qiu, Y.-P. Jiang, Q.-X. Liu, X.-G. Tang, Q.-J. Sun, Y.-C. Zhou and J.-M. Fan, *ACS Appl. Mater. Interfaces*, 2024, **16**, 31348–31362.
182 X. Ren, X. Wang and C. Jin, *Nano Lett.*, 2019, **19**, 8581–8589.

183 T. Sun, F. Yu, X. Tang, H. Li, F. Zhang, Z. Xu, Q. Liao, Z. Yu, X. Liu and P. Wangyang, *J. Materiomics*, 2024, **10**, 440–447.
184 G. Murastov, E. Bogatova, K. Brazovskiy, I. Amin, A. Lipovka, E. Dogadina, A. Cherepnyov, A. Ananyeva, E. Plotnikov and V. Ryabov, *Biosens. Bioelectron.*, 2020, **166**, 112426.
185 X. Chen, S. M. Shinde, K. P. Dhakal, S. W. Lee, H. Kim, Z. Lee and J.-H. Ahn, *NPG Asia Mater.*, 2018, **10**, 810–820.
186 T. Zhang, Y. Wan, H. Xie, Y. Mu, P. Du, D. Wang, X. Wu, H. Ji and L. Wan, *J. Am. Chem. Soc.*, 2018, **140**, 7561–7567.
187 C. Deng, L. Ren, L. Yang, X. Liu, Y. Dai, J. Zhao and T. Yue, *Environ. Sci.: Nano*, 2024, **11**, 278–293.
188 M. G. Vervloet, S. Sezer, Z. A. Massy, L. Johansson, M. Cozzolino, D. Fouque and ERA–EDTA Working Group on Chronic Kidney Disease–Mineral and Bone Disorders and the European Renal Nutrition Working Group, *Nat. Rev. Nephrol.*, 2017, **13**, 27–38.
189 L. Peng, N. Abbasi, Y. Xiao and Z. Xie, *Adv. Mater. Interfaces*, 2020, **7**, 2001538.
190 S. Adomavičiūtė-Grabusovė, A. Popov, S. Ramanavičius, V. Šablinskas, K. Shevchuk, O. Gogotsi, I. Baginskiy, Y. Gogotsi and A. Ramanavičius, *ACS Nano*, 2024, **18**(20), 13184–13195.
191 E. A. Vogler, *Biomaterials*, 2012, **33**, 1201–1237.
192 G. Guan, S. Zhang, S. Liu, Y. Cai, M. Low, C. P. Teng, I. Y. Phang, Y. Cheng, K. L. Duei and B. M. Srinivasan, *J. Am. Chem. Soc.*, 2015, **137**, 6152–6155.
193 X. Wu, F. Tan, S. Cheng, Y. Chang, X. Wang and L. Chen, *Nanoscale*, 2022, **14**, 3777–3787.
194 K. C. Mei, P. M. Costa, M. Kreuzer and K. T. Al-Jamal, *Adv. Mater. Interfaces*, 2021, **8**, 2100251.
195 M. Aleemardani, P. Zare, A. Seifalian, Z. Bagher and A. M. Seifalian, *Biomedicines*, 2021, **10**, 73.
196 T. A. Tabish, S. Zhang and P. G. Winyard, *Redox Biol.*, 2018, **15**, 34–40.
197 M. Maruthupandy, M. Rethinasabapathy, S. Jeon, J. Jeong, E. Kim, S. Lee, S. Kim, G. Kim, Y. Ha and E. Bae, *Nano Today*, 2023, **51**, 101925.

